MODELING OF CUTTING FORCES IN MICRO MILLING INCLUDING RUN-OUT

A THESIS
SUBMITTED TO THE DEPARTMENT OF MECHANICAL ENGINEERING
AND THE GRADUATE SCHOOL OF ENGINEERING AND SCIENCE
OF BILKENT UNIVERSITY
IN PARTIAL FULFILLMENT OF THE REQUIREMENTS
FOR THE DEGREE OF
MASTER OF SCIENCE

By
Muammer Kanlı
August, 2014

I certify that I have read this thesis and that in my opinion it is fully adequate, in scope and in quality, as a thesis for the degree of Master of Science.

Asst. Prof. Dr. Yiğit Karpat (Advisor)

I certify that I have read this thesis and that in my opinion it is fully adequate, in scope and in quality, as a thesis for the degree of Master of Science.

Asst. Prof. Dr. Melih Çakmakcı

I certify that I have read this thesis and that in my opinion it is fully adequate, in scope and in quality, as a thesis for the degree of Master of Science.

Asst. Prof. Dr. Hakkı Özgür Ünver

Approved for the Graduate School Of Engineering And Science:

Prof. Dr. Levent Onural
Director of the Graduate School

ABSTRACT

MODELING OF CUTTING FORCES IN MICRO MILLING INCLUDING RUN-OUT

Muammer Kanlı
M.S. in Mechanical Engineering
Supervisor: Asst.Prof.Dr. Yiğit Karpat
August, 2014

Micro milling is widely used in precision manufacturing industry which is suitable for producing micro scale parts having three dimensional surfaces made from engineering materials. High material removal rate is its main advantage over other micro manufacturing technologies such as lithography, micro EDM, laser ablation etc. Modeling of micro milling process is essential to maximize material removal rate and to obtain desired surface quality at the end of the process.

The first step in predicting the performance of micro milling process is an accurate model for machining forces. Machining forces are directly related to machine tool characteristics where the process is performed. The spindle and the micro milling tool affects the machining forces. In this thesis, the influence of runout of the spindle system on micro milling forces is investigated. Two different spindle systems with different levels of runout are considered and necessary modifications are introduced to model the trajectory of the tool center for better prediction of process outputs in the presence of runout. A modified mechanistic force modeling technique has been used to model meso/micro scale milling forces. Detailed micro milling experiments have been performed to calculate the cutting and edge force coefficients for micro end mills having diameters of 2, 0.6, and 0.4 mm while machining titanium alloy Ti6AL4V. Good agreements have been observed between the predicted and measured forces. It is found that statically measured runout values do not translate into dynamic machining conditions due to machining forces acting on the end mill.

Keywords: micro milling, cutting forces, run-out, trochoidal tool path

ÖZET

SALGILI MİKRO FREZELEMEDE KESME KUVVETLERİNİN MODELLENMESİ

Muammer Kanlı
Yüksek Lisans, Makina Mühendisliği
Tez yöneticisi: Asst.Prof.Dr. Yiğit Karpat
Ağustos, 2014

Mikro frezeleme, mühendislik malzemelerini kullanarak üç boyutlu yüzeylere sahip mikro ölçekli parça üretimi için uygun bir imalat yöntemidir ve hassas işlem endüstrisi tarafından sıklıkla kullanılmaktadır. Diğer mikro imalat tekniklerine (litografi, mikro EDM, lazer ablasyon vb.), göre en büyük avantajı yüksek talaş miktarına sahip olmasıdır. Talaş miktarını maksimize etmek ve işlem sonunda istenen yüzey kalitesine ulaşmak için mikro frezeleme işleminin modellenmesi gerekmektedir.

Mikro frezeleme işlem performansını öngörebilmenin ilk adımı kesme kuvvetlerinin doğru bir şekilde modellenmesidir. Kesme kuvvetleri, doğrudan işlemin gerçekleştiği tezgah parametrelerine bağlıdır. Ayna ve mikro freze çakısı kesme kuvvetlerini etkiler. Bu tezde, ayna sistem salgısının mikro frezeleme kuvvetleri üzerindeki etkisi incelenmiştir. Değişik miktarda salgıları olan üç farklı ayna sistemi düşünüldü ve salgılı bir sistemde proses çıktısını daha iyi öngörebilme amacıyla takım merkez yörüngesini modellemek için gerekli değişiklikler yapıldı. Meso/mikro ölçekli frezeleme kuvvetlerini modellemek için modifiye edilmiş mekanistik kuvvet modelleme tekniği kullanıldı. 2, 0.6 ve 0.4 mm çapındaki mikro freze çakılarının kesme ve kenar kuvvet katsayılarını hesaplamak için kapsamlı mikro frezeleme deneyleri yapıldı. Öngörülen ve ölçülen kuvvetlerin uyum içinde olduğu gözlendi. Statik olarak ölçülen salgı değerlerinin dinamik kesme şartlarında kullanılamayacağı görüldü, ki bu durum muhtemelen freze çakısı üzerinde etkili olan kesme kuvvetlerinden kaynaklanmaktadır.

Anahtar sözcükler: mikro frezeleme, kesme kuvvetleri, salgı, trokoidal takım yolu

Acknowledgement

I would like express my gratitude to my advisor, Asst.Prof. Yiğit Karpat for his guidance and support throughout my thesis work.

I would like express my gratitude also to my previous advisor, Asst.Prof. Metin Yavuz, METU/ANKARA for his guidance and support in METU.

Several individuals provided advice and additional resources that were instrumental in the success of this thesis. I would like to thank Mustafa Kılıç (Machine tool technician) and Samad Nadimi Bavil Oliaei (Ph.D. candidate) for their support, encouragement and helpful suggestions throughout my research.

I wish to thank also National Nanotechnology Research Center (UNAM) and Advanced Research Laboratories (ARL) for their help in measurements of this study.

Last but not least, I would like to thank to my family and friends, for their love and encouragement.

Contents

List of Figures

List of Tables

Nomenclature

a	axial depth of cut
dF_{t_j}, dF_{n_j}	differential cutting forces in tangential and normal directions
dF_{x_j}, dF_{y_j}	differential cutting forces in x and y directions
F_t, F_n	milling forces in tangential and normal directions
$\overline{F_x}, \overline{F_y}$	average cutting forces in x and y directions
f	Feed
h_j	uncut chip thickness as a function of immersion angle and axial position
i	helix angle of the end mill
k_t, k_n	tangential and normal milling-cutting force coefficients for linear fit
k_{te}, k_{ne}	tangential and normal milling-edge force coefficients for linear fit
$k_{n0,n1,n2,n3}$	normal milling force coefficients for polynomial fit
$k_{t0,t1,t2,t3}$	tangential milling force coefficients for polynomial fit
N	number of teeth
ϕ	immersion angle measured clockwise from positive y axis to a reference flute (j-=0)
ϕ_j	immersion angle measured clockwise

ϕ_{st}, ϕ_{ex}	start and exit angle of the immersion
R	radius of cutter
R_0, γ_0	magnitude and angle of radial run-out
s_t	feed rate per tooth
t	uncut chip thickness as a function of immersion angle
x_k, y_k	x, y coordinates of k^{th} tool tip trajectories
x	feeding direction, coordinate axis
y	normal direction, coordinate axis
z	axial direction, coordinate axis

Chapter 1

Introduction

Metal cutting is one of the most important manufacturing processes to obtain a part with the desired shape and dimensions by removing unwanted materials in the form of chips [1]. Different metal cutting operations have been developed for various applications including turning, drilling, boring, grinding and milling. Among these operations, milling operations has been widely employed to obtain three dimensional geometries and free form surfaces. Conventional milling process has been studied through experimental and analytical techniques; as a result higher productivity has been obtained. However, as for micro milling, better understanding of the process and reliable machining models are still lacking.

The drive for miniaturization still continues. The surface-to-volume ratio of miniature components is very high and hence consumes less power and transfer heat at a higher rate. To produce such components, micro milling is one of the fabrication technologies, which is widely used in the precision manufacturing industry for telecommunications, portable consumer electronics, defense and biomedical applications and is much more suitable for producing complex 3-D micro-structures.

Cutting force models are an essential part of the modeling efforts for the conventional and micro milling processes used to calculate milling power consumption, prediction of stable (chatter free) machining conditions, determining surface location errors and design of machine tools and cutting tools [1]. Three

different approaches are generally used for the modeling of cutting forces in milling, such as analytical, numerical and mechanistic. Analytical models are put forward through various scientific branches and designed to estimate the cutting forces. They also provide intermediary quantities such as stresses, strains, etc. The multiphysical process is fit by employing some number of empirical or statistical results. Numerical methods can be used to find the cutting forces directly by finite element simulation of milling. According to mechanistic (empirical) models, cutting and edge forces on the cutting tool face are regarded as the effective forces in the process. Cutting and edge forces constitute the resultant force. The former is related with the bulk shearing of the workpiece material in a narrow "shear" zone together with a friction at the tool-chip interface while the latter comes from rubbing and ploughing at the cutting edge. A set of slot milling experiments at different feeds and cutting speeds for a given cutting tool-material pair needs to be conducted. Different functions are fit to the experimental model to relate machining forces to cutting and edge coefficients.

For micro milling, some issues which are usually neglected in macro scale modeling must be taken into account. These are: i) minimum uncut chip thickness which defines the limit between ploughing and shearing, ii) runout on spindle system, which is due to inaccuracy of rotating parts in a mechanical systems, iii) delicate nature of micro end mills which wear out quickly especially when difficult-to-cut materials are machined. The focus of this thesis is the run-out in spindle systems and its influence on the machining forces.

Various runout models have been proposed in the literature. The proposed models have been investigated and then one of them is integrated into milling model. For further investigation, two different spindle systems are considered. Identical micro milling tests are conducted on two different spindles to observe the differences caused by spindle systems. First spindle system is a special one designed for micro milling and it has a low runout. The second one is a general purpose spindle which of its kinds is generally used in micro milling in practice.

Micro milling forces are modeled using a mechanistic force model which employs a third order polynomial used to relate machining forces to tangential and radial cutting forces acting on the micro tool.

The chapters of the thesis are organized as follows:

In Chapter 2, general milling force modeling is presented. Literature on modeling of cutting forces of milling is reviewed. The uncut chip thickness is calculated based on circular tool path assumption. Milling experiments with 2 mm diameter end mill are conducted. The simulation and experimental milling force measurement results are discussed.

The modeling of micro milling with tool run-out is investigated in Chapter 3. Trochoidal tool path assumption is used, which gives more accurate results compared to circular tool path assumption. The static run-out is measured and run-out parameters are extracted from the measurements. A comparison between the results of simulations and experiments is made and the limitations of the developed model are discussed.

In Chapter 4, the modeling of micro milling for spindles with large run-out is investigated. The milling forces are obtained and compared with the previous chapter.

Chapter 5 is devoted to the conclusions of this thesis together with a brief summary of contributions and suggestions for future work.

Chapter 2

Mesoscale Modeling of Milling Forces

2.1 Overview

The reliable data and equations for machining performance measures and their effect on the economic performance of the machining processes have long been noticed by researchers and practicing engineers. It has also been observed that the maximization of the performance comes not only from predicting and improving studies with optimization strategies, but the numerous influencing variables and wide range of different machining operations has to be considered.

In this respect conventional (macro) milling has long been studied by many scientists to explore the relations between the machining parameters (cutting speed, feed) and the outcomes (throughput, quality of machined surface, cutting tool's wear) which by time has made the milling process very efficient.

Dynamic milling forces can be established as explicit functions of cutting conditions and tool/workpiece geometry. Using one of the local cutting force model (linear or non-linear), three cutting process component functions can be created: basic cutting function, chip width density function and tooth sequence function. Basic cutting function establishes the chip formation process in the elemental

cutting area. Chip width density function outlines chip width per unit cutter rotation along a flute within the axial depth of cut. Tooth sequence function characterizes the spacing between flutes in addition to their cutting sequence as the cutter rotates. The cutting forces can then be constituted in the Fourier domain by the frequency multiplication of the transforms of these three component functions. Wang et al. investigated this subject and demonstrated that Fourier series coefficients of the cutting forces can be shown to be explicit algebraic functions of various tool parameters and cutting conditions [2].

In the following section, a literature survey related to force modeling of milling operation is presented, which is valid both for conventional or micro milling processes. Some exceptional features of micro milling that have to be concerned with will be examined in chapter 3.

2.2 Literature Survey

In historical respect, the force modeling for cutting process was first attempted by Martellotti [3]. He used an expression of $t = s_t \sin \phi$ for the basic cutter-chip thickness relationship. Here, t is the uncut chip thickness, s_t is the feed rate per tooth and (ϕ) is the immersion angle that orientates the cutter. By this formula, the milling cutter tool path was assumed to be circular instead of the real tool path, which is trochoidal. Although this is not an exact solution for the chip load, it gives a very good approximation when the feed rate per tooth is much less than the cutter diameter. Since then, this assumption has been widely used for the milling process modeling. Tlusty and MacNeil [4] set forth closed-form expressions for the milling force. They assumed a circular tool path and a constant proportionality between the cutting force and uncut chip thickness. Usui et al. has used energy method to model the chip forming and to predict three dimensional cutting forces by using only the orthogonal cutting data [5,6]. They applied the method to oblique cutting, plain milling and groove cutting operations. DeVor et al. assumed the cutting forces to be directly proportional to the uncut chip thickness in their paper [7,8] that made them the first to propose a mechanical model of cutting force in peripheral milling. Fu et al. developed a mechanistic model predicting the cutting forces in face milling over a range of cutting states,

cutter geometries and process geometries including relative positions of cutter to workpiece, spindle tilt and run-out [9]. Empirical coefficient obtained from fly-cutting and multi-tooth cutting tests were used to predict the milling forces. The measured forces have verified the model's prediction capability.

Armarego and Deshpande have predicted the average and fluctuating force components and torque in end milling [11]. They considered the 'ideal' model for rigid cutters with no eccentricity, the rigid cutter 'eccentricity' model and a more comprehensive 'deflection' model allowing for both eccentricity and cutter deflections. These three models showed different trends for the predictions of the average and fluctuating force components and torque. Montgomery and Altintas [12] developed the mechanistic model further by trochoidal tool path and predicted the cutting forces and surface finish under dynamic cutting conditions quite well.

The analytical cutting force of conventional end mill process was expressed as a function of chip thickness and cutting force coefficients, given by Eq. (1);

$$\begin{aligned} F_t &= \left(k_{te} + k_t t\right) z \\ F_n &= \left(k_{ne} + k_n t\right) z \end{aligned} \tag{1}$$

where $t = s_t \sin \phi$ and z is the width of the chip. This model has been further analyzed in detail by Budak et al. [1] where the cutting forces are separated into edge or ploughing forces and shearing forces that are calculated for small differential oblique cutting edge segments. This method is used by our analysis. Using mechanistic approach they determined milling force coefficients (i.e., shear angle, friction coefficient and yield shear stress) from orthogonal cutting experiments and used the oblique cutting analysis model developed by Armarego and Deshpande [13] to predict milling process forces. Armarego et al. have established a further step on a scientific, predictive and quantitative basis by using the mechanics of cutting approach and including many tool and process variables as well as the tooth run-out [14]. This model has been verified by simulations and experiments. Proven qualitatively and quantitatively, it has emphasized the effect of tooth run-out on the force fluctuations.

Lee and Altintas [15] developed the mechanics of cutting with helical ball-end mills by this method described in [1]. They validated this approach experimentally. Armarego presented the series of continuing researches that led to "Unified-Generalized Mechanics of Cutting Approach" in [16] to predict and model various machining processes. This approach elaborated the generalized mechanics of cutting processes with single edge or multi edge tools and the formation of a generic database of basic cutting and edge force coefficients. With these cutting analysis and database, a modeling methodology was shown for each machining operation.

For the prediction of cutting forces in milling, boring, turning and drilling with inserted tools Kaymakci et al. developed a unified cutting mechanics [19]. ISO tool standards were used to define the inserts mathematically. The material and insert geometry-dependent friction and normal forces were transformed into reference tool coordinates using a general transformation matrix. The forces, then were further transformed into boring, drilling and milling coordinates. The model was validated by experiments. The simulation of part machining with multiple operations and various tools can be achieved by this generalized modeling of metal cutting operations.

Kumanchik et al. [17] developed an analytical formula for the uncut chip thickness by considering the trochoidal tool path, run-out and uneven tooth spacing. The equation was generalized by combining the cutting parameters of milling (linear feed, tool rotational speed and radius) into a single, non-dimensional parameter. This enabled the milling process to be abstracted and allowed selecting the maximum possible chip thickness in milling. Time domain simulations showed lower error levels of the chip thickness values for this method, when it was compared with other commonly used methods.

Schmitz et al. investigated the effect of milling cutter teeth run-out on surface topography, surface location error and stability in end milling [18]. Arising from run-out, the periodically varying chip load on individual cutting teeth affects the milling process. By experiments they isolated this effect on cutting force and surface finish for various tooth spacing. Time domain simulations were verified by the tests. Relationships between run-out, surface finish, stability and surface location error were developed via simulation.

Cutting forces in machining operations can be found through various methods, namely analytical, numerical and mechanistic.

Analytical models are derived from the mechanics, material science and physics and designed to estimate the cutting forces. They provide intermediary quantities such as stresses, strains, etc. To fit the multiphysical process, milling some number of empirical or statistical results are employed.

Numerical methods can be used to find the cutting forces directly. By finite element method approach considering the milling as large deformation process cutting forces, chip flow and tool temperature distribution can be predicted. The effect of cutting conditions on stresses can also be studied with this method. But FEM-based simulations require the parameters of material flow characteristics at high temperature and deformation rates.

In mechanistic (empirical) cutting force models, cutting and edge forces are considered to be effective in the process. The cutting force is related with the bulk shearing of the workpiece material in a narrow “shear” zone together with a friction at the tool chip interface while the edge force comes from rubbing and ploughing at the cutting edge. Both constitute the resultant force. In this technique the effects of process variables (e.g., feed, depth of cut, cutting speed) are related to the experimentally measured average force components with the help of curve fitted equations. By the average forces, the specific cutting coefficients are calculated. The instantaneous cutting forces can then be specified with these coefficients. Very accurate results can be obtained with this simulation technique. But it requires testing for various cutting conditions; such as tool-workpiece couples, spindle speeds, depth of cuts.

2.3 Cutting Force Model For Milling Process

Figure 2.1 represents cutting forces acting on the tool during milling process. Tangential forces (F_t) are directed in the opposite direction of cutting velocity, and radial forces (F_n) are directed towards the center of the tool.

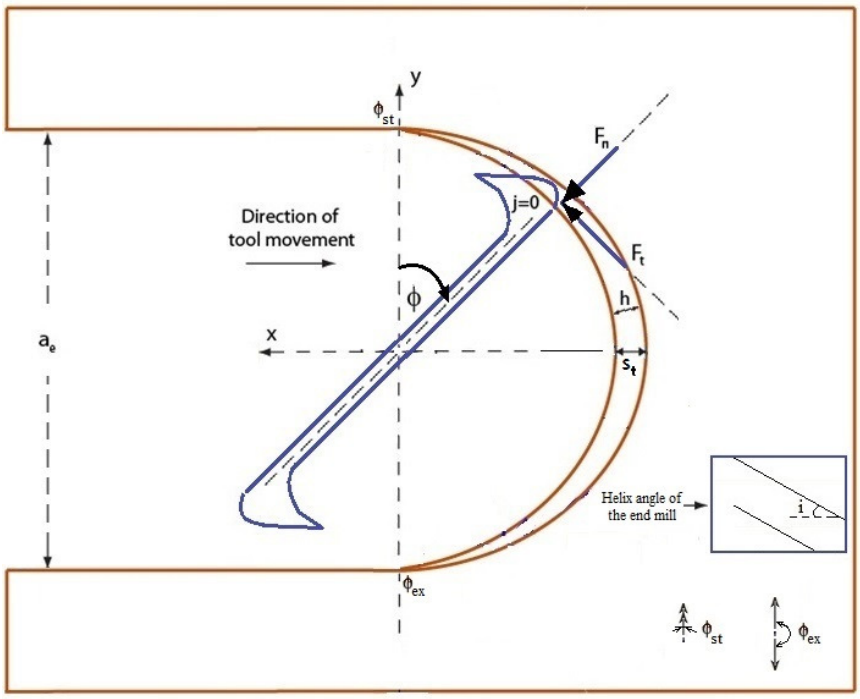

Figure 2.1: Milling forces and uncut chip thickness.

The differential force elements in x and y directions for an individual tooth can be obtained by considering axis transformation from n, t to x, y axes as shown in Eq. (2).

$$\begin{aligned} dF_{x_j} &= dF_{t_j}\cos\phi + dF_{n_j}\sin\phi \\ dF_{y_j} &= dF_{t_j}\sin\phi - dF_{n_j}\cos\phi \end{aligned} \tag{2}$$

The basic tangential and radial cutting forces acting on flute j of the model with a rigid cutter and zero eccentricity in the cutter rotation axis can be specified by Eq. (1), which was already given. Its differential form can be written as Eq. (3):

$$\begin{aligned} dF_{t_j} &= (k_{te} + k_t h_j)dz \\ dF_{n_j} &= (k_{ne} + k_n h_j)dz \end{aligned} \tag{3}$$

where h_j, the uncut chip thickness is a function of immersion angle (ϕ) and axial position (z). Here; k_t, k_n are the cutting force coefficients and k_{te}, k_{ne} are the edge force coefficients in tangential and normal directions, respectively. Then, substituting Eq. (3) into Eq. (2) yields Eq. (4).

$$\begin{aligned} dF_{x_j} &= \left[k_{te}\cos\phi_j + k_{ne}\sin\phi_j + (k_t\cos\phi_j + k_n\sin\phi_j)h_j\right]dz \\ dF_{y_j} &= \left[k_{te}\sin\phi_j - k_{ne}\cos\phi_j + (k_t\sin\phi_j - k_n\cos\phi_j)h_j\right]dz \end{aligned} \tag{4}$$

Uncut chip thickness is calculated based on circular tool path assumption where $h_j = s_t \sin\phi(z)$ (s_t: feed rate per tooth). Figure 2.2 illustrates the variation of the chip thickness as a function of tool rotation angle for a milling tool having two teeth.

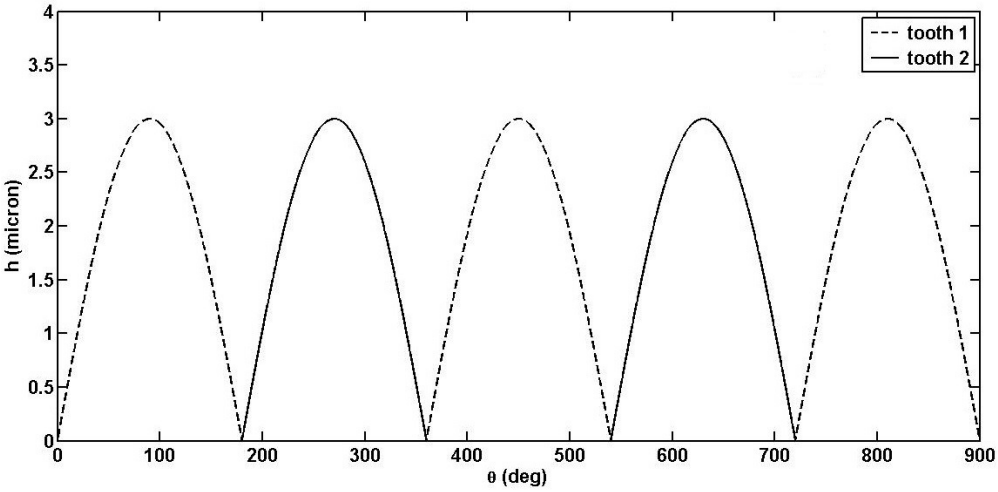

Figure 2.2: Uncut chip thickness variation
for circular tool path for 3 μm feed per tooth.

Considering $\phi_j(z) = \phi + \left(\frac{2\pi}{N}\right)j - \left(\frac{\tan i}{R}\right)z$ and integrating dF_{x_j} and dF_{y_j} with respect to z result in Eq. (5):

$$\begin{aligned} \int dF_{x_j} &= \frac{R}{\tan i}\left[-k_{te}\sin\phi_j + k_{ne}\cos\phi_j + \frac{s_t}{4}\left[k_n(-2\phi_j + \sin 2\phi_j) + k_t\cos 2\phi_j\right]\right]_{z_{j,1}(\phi)}^{z_{j,2}(\phi)} \\ \int dF_{y_j} &= \frac{R}{\tan i}\left[k_{te}\cos\phi_j + k_{ne}\sin\phi_j + \frac{s_t}{4}\left[k_t(-2\phi_j + \sin 2\phi_j) - k_n\cos 2\phi_j\right]\right]_{z_{j,1}(\phi)}^{z_{j,2}(\phi)} \end{aligned} \tag{5}$$

Then the average force can be calculated by integration as follows:

$$\overline{F_x} = \frac{1}{2\pi}\int_0^{2\pi}\left\{\sum_{J=0}^{N-1}\frac{R}{\tan i}\left[\begin{array}{l}-k_{te}\sin\phi(z)+k_{ne}\cos\phi(z)-\\ \frac{s_t}{4}\left[k_n(2\phi(z)-\sin 2\phi(z))-k_t\cos 2\phi(z)\right]\end{array}\right]_{z_{j,1}(\phi)}^{z_{j,2}(\phi)}\right\}d\phi$$

$$\overline{F_y} = \frac{1}{2\pi}\int_0^{2\pi}\left\{\sum_{J=0}^{N-1}\frac{R}{\tan i}\left[\begin{array}{l}k_{te}\cos\phi(z)+k_{ne}\sin\phi(z)-\\ \frac{s_t}{4}\left[k_t(2\phi(z)-\sin 2\phi(z))+k_n\cos 2\phi(z)\right]\end{array}\right]_{z_{j,1}(\phi)}^{z_{j,2}(\phi)}\right\}d\phi \quad (6)$$

, where it must be noticed that;

- For each tooth, the same magnitude dF_{x_j} applies, i.e. the summation over N tooth is equivalent to multiplication of dF_{x_j} with N,
- For $\int dF_{x_j}$, ϕ is assumed to be constant,
- Either $\left(z_{j,2}(\phi), z_{j,1}(\phi)\right)$ or $\left(\phi_{ex}, \phi_{st}\right)$ can be used as the boundary,
- The signs are changed because $\overline{F_{x,y,z}}$'s are to be measured by a dynamometer, making it in the opposite direction.

Then the average forces in x,y direction can be found to be as in Eq. (7).

$$\overline{F_x} = \frac{aN}{2\pi}\left[k_{te}\sin\phi - k_{ne}\cos\phi + \frac{s_t}{4}\left[-k_t\cos 2\phi + k_n(2\phi - \sin 2\phi)\right]\right]_{\phi_{st}}^{\phi_{ex}}$$

$$\overline{F_y} = \frac{aN}{2\pi}\left[-k_{te}\cos\phi - k_{ne}\sin\phi + \frac{s_t}{4}\left[k_t(2\phi - \sin 2\phi) - k_n\cos 2\phi\right]\right]_{\phi_{st}}^{\phi_{ex}} \quad (7)$$

, where $a = \dfrac{(\phi_{ex} - \phi_{st})R}{\tan i}$

Here, by defining the following set of equations;

$$P = \frac{aN}{2\pi}\left[\cos 2\phi\right]_{\phi_{st}}^{\phi_{ex}} \qquad Q = \frac{aN}{2\pi}\left[2\phi - \sin 2\phi\right]_{\phi_{st}}^{\phi_{ex}}$$

$$S = \frac{aN}{2\pi}\left[\sin\phi\right]_{\phi_{st}}^{\phi_{ex}} \qquad T = \frac{aN}{2\pi}\left[\cos\phi\right]_{\phi_{st}}^{\phi_{ex}} \quad (8)$$

the average forces can be simplified as below:

$$\overline{F_x} = k_{te}S - k_{ne}T + \frac{s_t}{4}\left(-k_t P + k_n Q\right) \qquad \overline{F_y} = k_{te}T - k_{ne}S + \frac{s_t}{4}\left(k_t Q + k_n P\right) \tag{9}$$

Then k_{te}, k_t, k_{ne} and k_n can be found by P, Q, S, T of Eq. (8), respectively as follows:

$$k_{te} = \frac{\overline{F_{xe}}S - \overline{F_{ye}}T}{S^2 + T^2} \qquad k_t = 4\frac{\overline{F_{yc}}Q - \overline{F_{xc}}P}{P^2 + Q^2}$$
$$k_{ne} = \frac{k_{te}S - \overline{F_{xe}}}{T} \qquad k_n = \frac{k_t P + 4\overline{F_{xc}}}{Q} \tag{10}$$

These cutting coefficients represent materials' resistance to machining as a function of tool geometry and tool material: k_t, k_n are due to shearing at the shear zone and friction at the rake face, while k_{te}, k_{ne} are due to rubbing or plowing at the cutting edge. In order to be able to calculate cutting and edge force coefficients from Eq. (10), one must conduct slot milling experiments at various feed rates. Eq. (3) represents a linear equation where in parenthesis the first term represents the intercept value on the y-axis and the second term includes the slope. The average forces calculated in x and y direction under at least three feed rates can be used to find the slope and intercept values which are in turn used to calculate the unknown cutting force and edge coefficients.

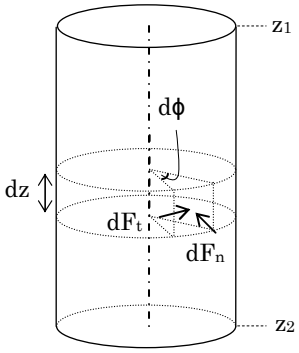

Figure 2.3: Elemental milling forces in tangential and normal directions on finite cutting zone

Briefly, till now it is shown that the milling force coefficients, k_{te}, k_t, k_{ne}, k_n can be calculated from the experimental force results that were obtained in slot

milling tests. By using these coefficients, Eq. (3) is used to find the elemental tangential and normal forces in finite elements of the miling tool, obtained by discretization of the cutting area, as shown in Figure 2.3. These forces are transformed into x, y coordinates by Eq.(2). These elemental cutting forces are then summed up along z, ϕ and number of teeth.

2.4 Experimental Setup

In this chapter, the milling experiments were performed on the three axis milling machine (DMG HSC 55, Figure 3.8) equipped with a maximum spindle speed of 18,000 rpm. It has X,Y,Z range of 450, 600, 400 mm, respectively.

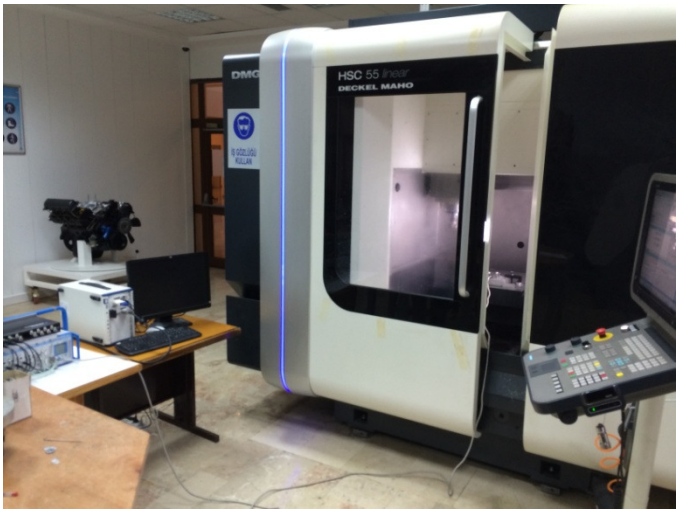

Figure 2.4: DMG HSC 55 three axis milling machine used in milling experiments.

In these experiments, slots are milled to obtain the cutting forces F_x and F_y, in x and y directions, respectively. A 50 mm diameter Ti circular disc is used as a workpiece. For these slots, an entrance channel of 0.4 mm depth and 4 mm width was machined. This makes the milling quicker to stabilize and the tool less prone to wear. WC flat end mill (NS Tool Co. [45], 2 teeth, 30° helix angle) of 2 mm diameter is used as the cutting tool (Figure 2.5).

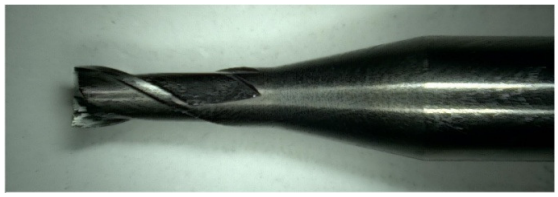

Figure 2.5: Flat end mills by NS Tools Co.

Micro machining forces are measured by Kistler mini dynamometer (9256C1, max 250 N) with its charge amplifier and transferred to a PC through a data acquisition card (National Instruments). The measurement setup is shown in Figure 2.6. To be able to obtain enough data to observe the real force trends in the milling experiments, measuring frequency of the dynamometer was specified to be 10^5 Hz. All experiments are performed under dry machining conditions.

Figure 2.6: Measurement setup.

Two different cutting speeds were experimented. Table 2.1 shows the preliminary experimental conditions used in this study.

Table 2.1: Experimental Milling Conditions.

Tool Diameter (mm)	**Spindle Speed (rpm)**	**Cutting Speed (m/min)**	**Depth of Cut (µm)**	**Feed Rate, (µm /tooth)**
2	10,000	62.8	200	2-4-6-8-12-18
2	14,000	88.0	200	6-12-18

Each milling test was performed on fresh cutting tool. So the effect of wear on the forces can be ignored. To exclude the dynamic effects of spindle, the force data taken by the measurement setup was digitally filtered by low pass filter (IIR) of the frequency calculated by rpm*4/60, which gives filter magnitudes of 667 and 933 hz for 10,000 and 14,000 rpm, respectively. To take a satisfactory average force, the steady state part of the cutting forces is selected to avoid the effect of distorted force signature because of tool impact at the beginning and end of cut. Therefore, cutting force data was cropped by checking the tendency of the test results. Generally 20 percent from the beginning and 10 percent from the ending part of the cutting force was ignored in calculations.

2.5 Calculation Of Cutting And Edge Coefficients

As shown in Figure 2.7 for a 2 mm diameter tool at 10,000 rpm, the average cutting forces increase as the feed/tooth rises up. Line fits can also be seen on the plot.

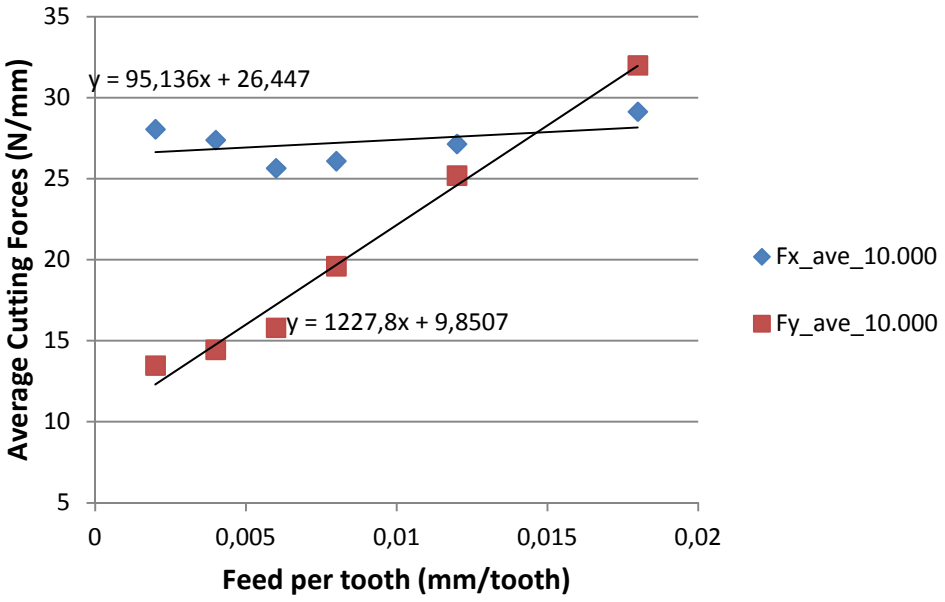

Figure 2.7: 10,000 rpm, 0.2 mm depth of cut, 2 mm diameter, Ti6Al4V.

Figure 2.8 shows the average force data for 14,000 rpm. The cutting and edge force coefficients for 10,000 and 14,000 rpm spindle speeds can be found in Table 2.2.

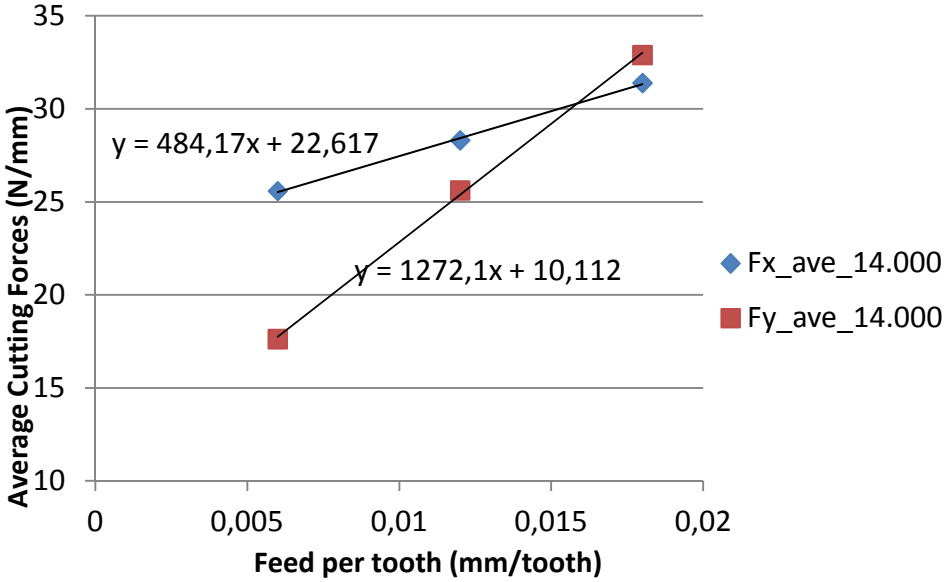

Figure 2.8: 14,000 rpm, 0.2 mm , 2 mm diameter, Ti6Al4V.

Table 2.2: Calculated cutting and edge force coefficients for 2 mm tool at two different speeds.

	k_{te} (N/mm²)	k_t (N/mm)	k_{ne} (N/mm²)	k_n (N/mm)
10,000 rpm	15.47	2455.6	41.54	190.27
14,000 rpm	15.88	2544.2	35.53	968.34

Based on the cutting and edge force coefficients given in Table 2.2, one can conclude that increasing cutting speed does not significantly change the cutting and edge coefficients in the tangential direction. However, increasing cutting speed yields larger cutting force coefficient and lower edge force coefficient in the radial direction. This may be related to complex interaction between the work and cutting tool flank surfaces.

Two plots in Figure 2.9 show the measured and calculated F_x and F_y forces during milling with a 2 mm diameter at 10,000 rpm with 4 μm feed/tooth and 200 μm depth of cut. Figure 2.10 shows the same data in chart form. It can be seen that under the given milling condition, force calculations using the model given above agree well with the measurements.

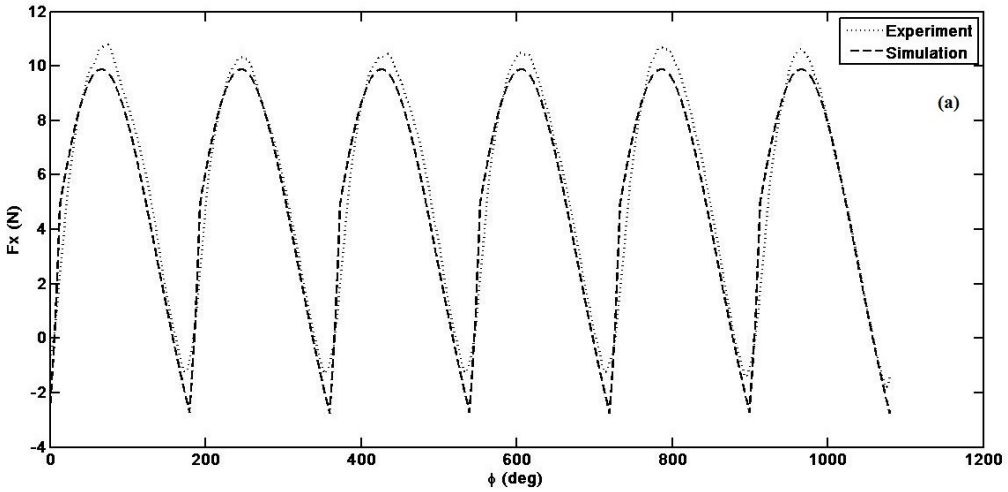

(a) F_x

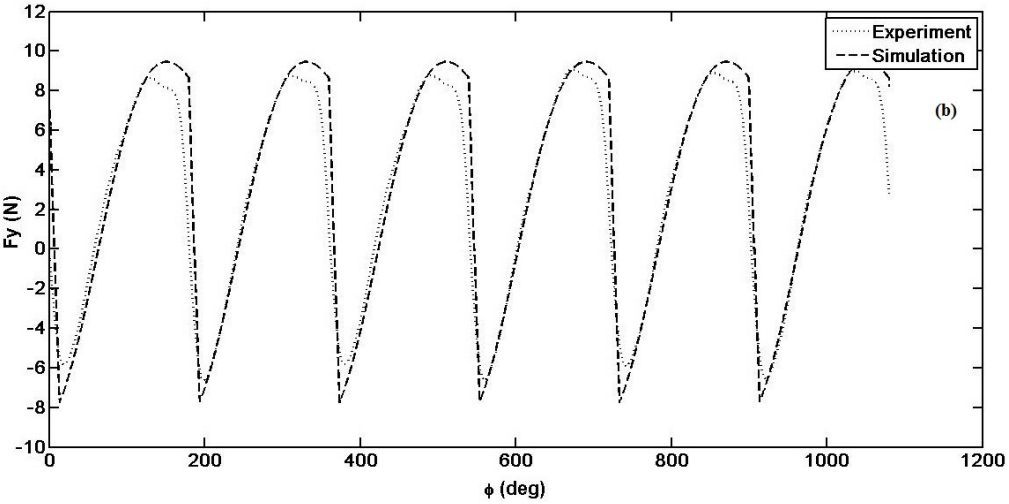

(b) F_y

Figure 2.9: Instantaneous milling force values measured and predicted for 10,000 rpm, 2 mm diameter cutting tool on Ti6Al4V workpiece with 0.2 mm depth of cut and 4 μm feed/tooth conditions;

The measured/modeled forces, especially the peak values seem to be quite periodic, which means that each tooth is facing with similar milling conditions.

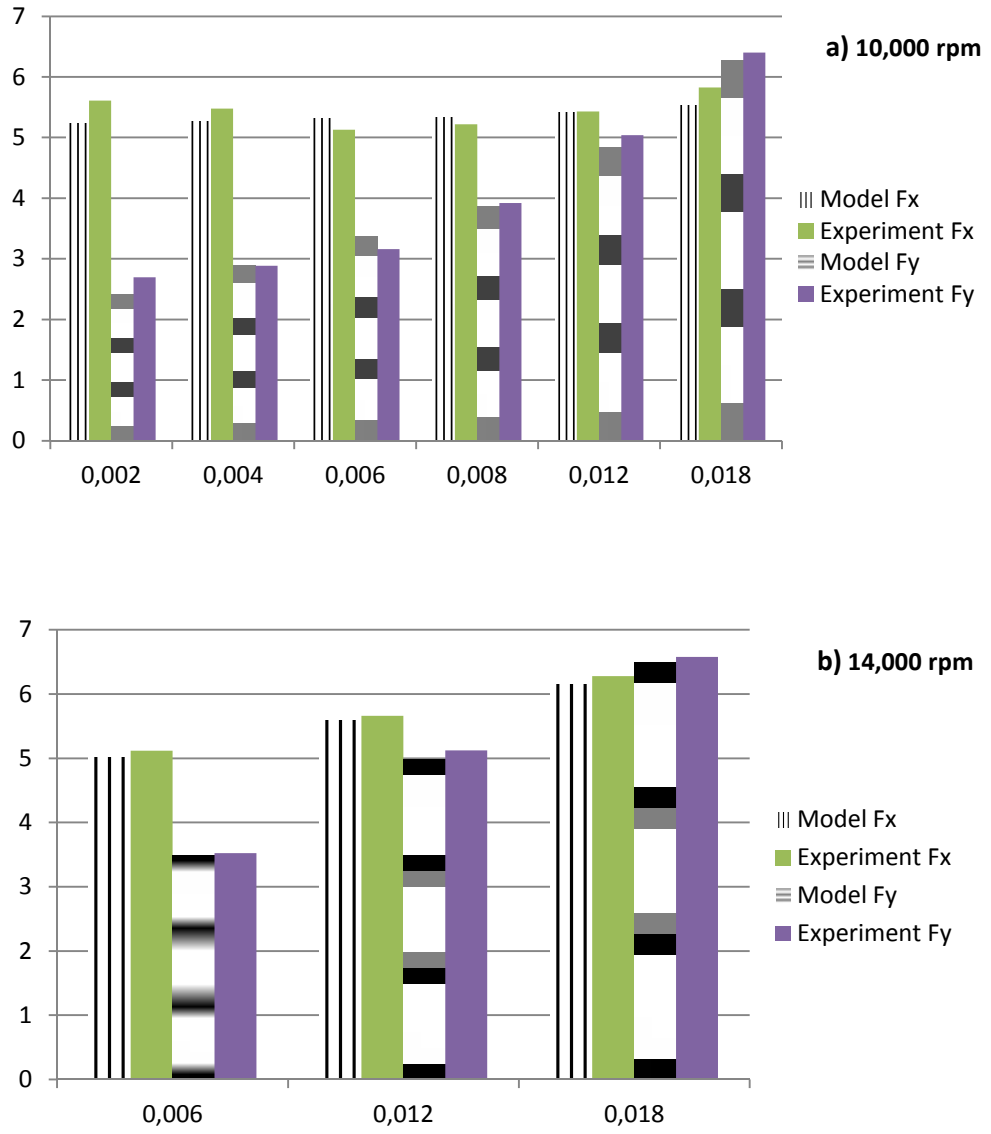

Figure 2.10: Average milling force values measured and predicted for 2 mm diameter cutting tool on Ti6Al4V workpiece with 0.2 mm depth of cut and various feed/tooth conditions.

Table 2.3: Errors in the average cutting force values for the model for 2 mm tool at 10,000 rpm speed and various **feed**/tooth milling conditions.

Feed rate (μm/tooth)		**Exp.**	**Model**	**Error (%)**
0.002	$\mathbf{F_x}$	5.61	5.23	-6.77
	$\mathbf{F_y}$	2.694	2.42	-10.17
0.004	$\mathbf{F_x}$	5.477	5.27	-3.78
	$\mathbf{F_y}$	2.888	2.9	0.42
0.006	$\mathbf{F_x}$	5.129	5.31	3.53
	$\mathbf{F_y}$	3.16	3.38	6.96
0.008	$\mathbf{F_x}$	5.217	5.34	2.36
	$\mathbf{F_y}$	3.92	3.87	-1.28
0.012	$\mathbf{F_x}$	5.428	5.42	-0.15
	$\mathbf{F_y}$	5.038	4.83	-4.13
0.018	$\mathbf{F_x}$	5.827	5.53	-5.10
	$\mathbf{F_y}$	6.399	6.28	-1.86

General trends of the experimental cutting force values can be sometimes misjudged by considering only the average force values. Alongside the error values of the average forces (Table 2.3), more reliable check is to be shown below.

Table 2.4: Errors in the peak instantaneous force values for the model for 2 mm tool at 10,000 rpm speed.

	1st tooth				**2nd tooth**			
	max F_x (N)		**max F_y (N)**		**max F_x (N)**		**max F_y (N)**	
	Exp.	**Simu.**	**Exp.**	**Simu.**	**Exp.**	**Simu.**	**Exp.**	**Simu.**
	10.807	9.816	9.062	9.397	10.332	9.816	8.782	9.397
Error,%	-9.17		3.7		4.99		7.00	

From Figure 2.9, a good verification of this model for calculation of instantaneous cutting forces, F_x and F_y with the 2 mm diameter cutting tool can be observed. Table 2.4 gives the errors in the peak instantaneous force values of the

model without run-out for 10,000 rpm speed. Errors of 9.17 % and 3.7 % are quite low values for milling force modeling.

2.5.1 High-presicion positioning subsystem

The meso scale milling model together with the identified cutting and edge force coefficients allows us to model the process well for 2 mm diameter end mills (Figure 2.9 and Table 2.4). In the next chapter, the milling model will be adapted to micro milling by including tool runout and trochoidal tool path.

Chapter 3

Micro Milling Modeling with Tool Run-out

3.1 Overview

While it can be regarded as the downscaled version of the conventional milling with end mills of sub-milimeter dimensions, micro milling has some distinct features that should be considered for more accurate process modeling when compared with conventional milling. These, actually come from miniaturization of the workpiece, tool and process. Small vibrations and excessive forces (compared to the micro-sized tool) affect tool endurance and component tolerances very much [37]. The size effect hinders also the detection of cutting edge damage and even tool shaft breakage. As a result, the cutting tool wears out in a quicker and undetectable manner, which becomes the major cause of lower component tolerance and broken tool shafts.

Micro milling requires micro tools and high-speed spindles. Therefore, tool manufacturing errors and tool alignment errors comes out to be relatively high compared to the associated chip load. Tool run-out can be considered as the total figure for these errors.

In macro milling, the cutting tool diameter is big and the run-out per tool diameter is very small. Therefore circular tool path assumption (Chapter 2) do not

give big error for the undeformed chip thickness, i.e. the basic variable for cutting force calculation. In micro milling however, because of the miniaturized dimensions and increased effect of the run-out this basic variable should be calculated more accurately. For that reason, trochoidal tool path model is used.

To investigate these distinguishing features, in this chapter micro milling process is modeled using another approach based on true tooth geometry and trochoidal tool path.

3.2 Literature Survey

In this section, the researches that have studied and explored the characteristics of micro milling are shown firstly. Then, those that have included the run-out effect are to be demonstrated.

Kim and Kim [22] offered a theoretical analysis for micro milling at very small depths of cut. They considered the elastic recovery of the workpiece and ploughing by the tool edge radius to be important in micro-cutting range. A special orthogonal cutting model, the so-called RECM (round-edge cutting model) was offered to take these two effects into account. While the bulk shearing of the workpiece material in a narrow shear zone affects the cutting forces primarily, the ploughing factor becomes noticable when the uncut chip thickness is of the order of cutting edge radius. Waldorf et al. [23] analyzed the ploughing component of cutting force for finishing conditions. To model this effect a slip-line field was developed, combining a small stable build-up of material sticked to the edge and a raised prow of material formed ahead of the edge. The relation between the ploughing forces and the cutter edge radius was shown to be as follows: a larger edge causes bigger ploughing forces. Their experiments with different edge radii and different levels of chip load have matched well with the proposed model's predictions.

In all of the above studies the milling process model was based on the customary circular tool path assumption. Putting a high degree of simplification for the analysis work, it brings about inevitable errors to the solutions, which cannot satify the increasing accuracy needs of ultra precision engineering.

Therefore many scientists [17, 18, 19] started to consider the true "trochoidal" tool path in their studies. With this regard, Bao and Tansel [24-26] studied the cutting force model of micro-end-milling operations with and without tool run-out, analytically. Their study was based on Tlusty et al.'s [4] model. Their experiments have shown that the new analytical cutting force model gave better cutting force predictions than the existing analytical model. The difference in the estimations increased for high ft/r (feed per tooth/edge radius) ratios. It was suggested that maximum cutting force expressions, variation of the cutting force in one complete rotation, surface quality and many other characteristics of the cutting force components can be derived from the proposed model. These variables can be calculated very quickly by these expressions compared to numerical simulation programs that calculate the cutting forces by evaluating the location of tool tip at the present and previous rotations. Charts of these results can be prepared to allow machining operators to easily select the cutting conditions [24]. Bao et al. included the tool run-out in the model in another paper [25]. Run-out inclusion has allowed the uncut chip thickness and cutting forces to be calculated even more accurately. They also offered compact expressions with optimization algorithms to estimate the tool run-out, machining parameters, surface quality, and tool conditions from the experimental cutting force data. Bao et al. considered the effect of tool wear, also [26].

As the depths of cut and feed rates are reduced, the chip load encountered in cutting process becomes the same order of magnitude as the grain size of many alloys. The workpiece material can be considered as homogeneous and isotropic for conventional milling processes. But for micro-milling applications the workpiece material must be modeled as heterogeneous and, in some cases, anisotropic. With this regard Vogler et al. developed a microstructure-level force prediction model for micro-milling of multi-phase materials [27].

Modeling the uncut chip thickness and cutting forces in a better way requires the deflection of milling tool to be incorporated. For small milling tools (diameter < 1mm) this fact becomes important. Dow et al. established a technique to compensate the tool deflection effect [28]. Being an open-loop technique, this predicts the cutting and thrust forces, applies these forces to the tool, calculates the shape error due to tool deflection and creates a new tool path to eliminate this

error. Minimum chip thickness (MCT) effect comes out into existence when the chip load is smaller than a fraction of the edge radius of the cutting tool in some extent, which is valid for micro milling operations where feeds per tooth are very low compared with the conventional milling practice. This effect causes the tool to uncut the workpiece unless the chip load is greater than a certain value that depends on some parameters like edge radius, workpiece-tool pairs, etc. This intermittent chip formation can be observed from the level of periodicity of cutting forces measured at various feeds per tooth. Concerning this subject, Kim et al. investigated the static model of chip formation in microscale milling and provided a method for predicting the minimum chip thickness and discussed on process parameter selection for intermittent-free chip formation [29].

To model the transient cutting forces correctly, it is required to determine the instantaneous uncut chip thickness (IUCT) precisely. Wan and Zhang introduced a method of calculation of IUCT and cutting forces in flexible end milling, which includes the cutter/workpiece deflections and the immersion angle variation [31]. Regeneration method was used to calculate IUCT and the numerical results were validated.

Chae et al. gave a good detailed review of micro-cutting operations [32]. Details of micro cutting (chip formation, cutting forces, tool wear, burrs), similarities and differences from macro-machining, cutting tools, machine tools, testing, handling, assembly issues, auxiliary processes, micro factories, possible application areas, recent research were prescribed in detail. Some recommendations about micro cutting operations were also given.

Dhanorker et al. introduced mechanistic and finite element modeling meso/micro end milling processes [33]. By considering the tool edge ploughing forces but ignoring the dynamics of tool-workpiece interaction they studied the effects of cutting conditions in cutting force and temperature distributions. The model was tested and verified for meso/micro milling of AL 2024-T6 aluminum.

Based on Tlusty et al.'s [4] cutting force model, Kang et al. studied the effect of tool edge radius through the analytic model [35]. The prediction was verified by the micro milling experiments on aluminum.

In micro-end milling, tool alignment errors and tool manufacturing errors like flute deviation and cutting edge offset play an important role because of their

large magnitude compared to related chip load and machined features. To characterize the effect of these errors on the machining accuracy and process performance two effective error parameters were defined by Jun et al., namely maximum radius of rotation (R_{cmax}) and difference in the radii of rotation (ΔR_c) [36]. The former was offered to be estimated from machined features while the latter was measured from acoustic emission signals during the process.

Lai et al. studied the following aspects of micro scale milling operation: its characteristics, size effect, micro cutter edge radius and minimum chip thickness [37]. The material strengthening behaviour at micron level was modeled with a modified Johnson-Cook constitutive equation by using strain graident plasticity. Finite element model for micro scale orthogonal machining process was elaborated considering the material strengthening behaviour, micro cutter edge radius and fracture behaviour of the work material. Then the cutting principles and the slip-line theory were used to develop an analytical micro scale milling force model. Results of OFHC (oxygen-free high thermal conductivity) copper micro milling experiments showed good agreements with the predicted results. Various research findings were observed: (1) minimum chip thickness is approx. 0.25 times of cutter edge radius for OFHC copper when the rake angle is 10° and the cutting edge radius is 2 μm. (2) The main cause of the size effect in micro miling is material strengthening behavior. (3) The ploughing phenomenon and the accumulation of the actual chip thickness are the primary causes for the large increase in specific shear energy when the chip thickness is smaller than minimum chip thickness.

Ber and Feldman made the earliest attempt on modeling the geometry for the radial and axial run-out of multi-tooth cutters [20]. Then Kline and Devor studied the effect of run-out due to cutter offset on cutting geometry and forces in end milling [21]. Having developed mathematical models, they found a significant change in the cutting force component at the spindle frequency caused by cutter offset. As mentioned in Chapter 2, Fu et al. proposed a force model for a face milling process with both radial and axial cutter run-out [9].

Being a common phenomenon in multi-tooth machining processes, cutter run-out may be originated from cutter axis offset, cutter axis tilt, errors in the grinding of the cutter, lack of dynamic balancing, irregularities in the cutter pockets, insert size, or the setting of the inserts. Since it causes the chip load to

vary over the rotation of the cutter, it influences the accuracy of the machined surface and the tool life in large extend. Li and Li investigated the effects of cutter run-out on milling process and proposed a new approach to model the geometry of the milling process with cutter run-out based on trochoidal tool path [30]. Instantaneous chip load, entry and exit angles of cutting tooth and ideal peripheral machined workpiece surface roughness are modeled. Incorporated into a predictive milling force model and verified by experiments, this study showed that the most important factor concerning the effects of run-out on the milling process geometry is the change of cutter radius for a tooth relative to the preceding tooth. Highest tooth enters the cut earliest and leave the cut latest and vice versa. This causes varied chip loads, which greatly affects the magnitudes and frequencies of the cutting forces.

Li et al. considered the combination of trochoidal trajectory of tool tip, tool run-out and minimum chip thickness effect and suggested a new nominal uncut chip thickness expression [34]. Because of the on-and-off nature of chip formation, elastic-plastic deformation regime and ploughing and shearing dominated chip formation regime were considered to constitute the micro milling process. Three dimensional cutting forces were calculated accordingly. The periodicity of cutting forces was found to be a function of minimum chip thickness and cutting conditions. The simulation results and experiments agreed quite well. It has also been suggested that tool breakage and wear can be predicted by inspection of the cutting force coefficients.

To explore the mechanistic modeling of micro milling forces Malekian et al. considered the effects of ploughing, elastic recovery, run-out and dynamics [38,39]. Based on the interference volume between the tool and the workpiece, a ploughing force model taking the elastic recovery effect into account was developed. Experimental scratch tests using a conical indenter diagnosed the elastic recovery. Due to the inconvenience of impact hammer testing for micro end mills, receptance coupling of the spindle/machining centre and the micro tool was employed to identify the dynamics at the tool tip. Receptance coupling can be defined as the mathematical coupling of the experimental dynamics with the analytical dynamics. Wide range of cutting conditions was experimented and the model was validated.

Wyen et al. investigated the influence of cutting edge radius and cutting speed on active milling force components, namely cutting force (F_c), feed force (F_f) , ploughing force (F_{Pl}) and coefficient of friction (μ) [40]. A method was offered for the characterization of rounded cutting edge. Experiments performed for various cutting edge radii and cutting speeds showed a number of trends that may be clarified by some physical explanation concerning the milling process.

Afazov et al. offered a new way for micro milling cutting forces calculation using finite element methods [41]. Taking run-out effect into account, the uncut chip thickness and the tool path trajectory were determined for distinct micro milling parameters (spindle speed, cutting tool radius, feed rate and number of teeth). An orthogonal FE model was elaborated and a number of FE analysis were made at different uncut chip thicknesses and velocities, through which the relation between cutting forces, chip load and cutting velocity has been described by a non-linear equation. This equation is a function of chip load and consists of linear and exponential portions, which calculates the ploughing and shearing dominant cutting forces, respectively. Then the cutting forces were predicted by putting the chip load calculated at the beginning into this non-linear force equation as an input. Comparison of the predicted and measured cutting forces showed quite good agreement.

Micro milling technology was explained in detail on a website based on a doctoral thesis [42]. Processes, machine tool, cutting tool and various applications of micro milling were explained.

Germain et al. have reviewed force prediction models proposed till now. Analytical and empirical models were indicated in detail [43]. Their differences concerning how and where to apply them and their performance for modeling the process were explained. As an example of comparison of analytical and mechanistic models, machining of CuC_2 pure copper was investigated. Mechanistic model was found to be more accurate.

3.3 Micro Milling Force Modeling Including Tool Run-Out

For macro (conventional) milling practice, the tool run-out has not big effect on the milling forces, as shown in the previous chapter. This comes from the fact that the tool diameter is big and the run-out is small in comparison to the tool diameter, which makes the run-out have very little effect on the undeformed chip thickness calculations. But for micro milling process both true tool path and run-out has to be considered if more accuracy in the cutting force calculation is demanded. Run-out has actually not only a profound effect on machined surface topography and stability of the micro milling process, but it also causes premature cutting edge failures. In this respect it must be explored and included in the cutting force predictions.

Tool run-out can be defined as the magnitude of the variation of tooth/insert radial location which varies periodically the chip load on the respective cutting tooth. As a result, the instantaneous cutting forces which have a direct relation with the chip load lose their periodicity. Therefore each tool faces with different milling condition. The “true” trajectory of the cutting edge depends on the feed rate, spindle speed, tool diameter and tool run-out.

As mentioned earlier, run-out is the common problem of micro milling. It can be specified with two components, namely angular run-out and radial run-out [44]. Angular run-out is the result of a misalignment between the rotational axis of the cutting tool and the central axis of the collet/spindle system as depicted in Figure 3.1. Radial run-out, which is determined by two parameters, (R_0, γ_0) is the result of the lateral offset between the rotational axis of the tool and the central axis of the collet/spindle system. Both combine to cause a cutting tool center offset.

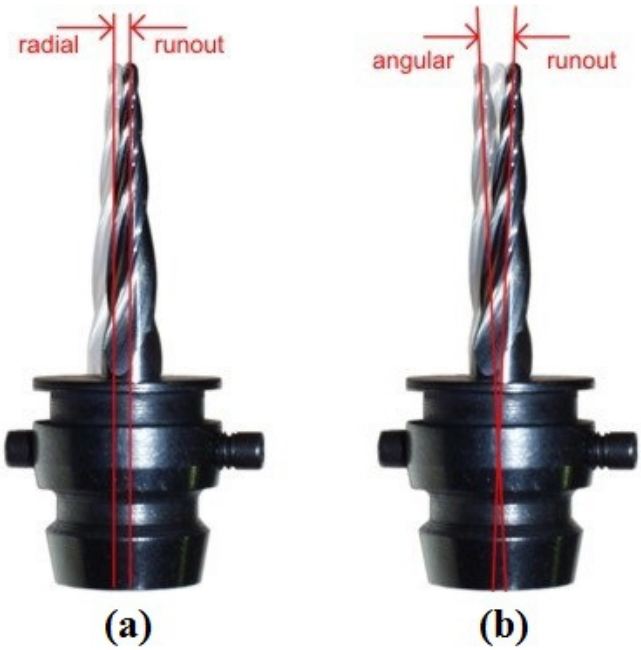

Figure 3.1: Angular (a) and radial (b) run-out description [44].

As can be seen in Figure 3.2, the tool cannot advance in a linear horizontal direction; it instead makes a trochoidal motion, because of the cutting tool center offset. The following expressions are adapted from Afazov's study [41].

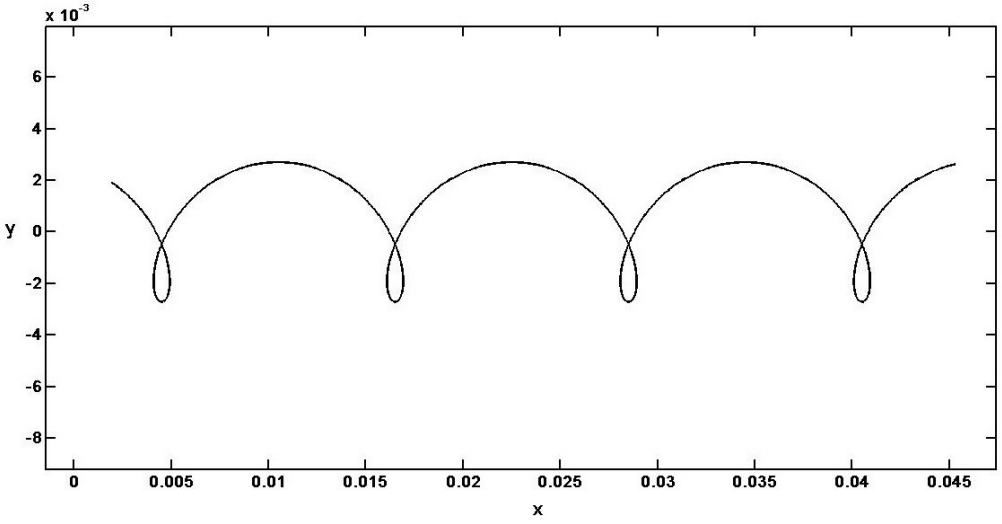

Figure 3.2: Real path of the cutting tool center.

The trajectory of k^{th} and $(k-1)^{th}$ teeth can be figured out as shown in Figure 3.2. It seems quite different from the previous model because both the tool center motion and the run-out are included into this model. The uncut chip thickness is calculated by using the paths of successive k^{th} and $(k-1)^{th}$ teeth. Considering run-out and trochoidal motion, the real tool path can be plotted as shown in Figure 3.3. Here (x',y') refers to the tip position of one of the tooth (in this model $(k-1)^{th}$) while the (x,y) refers to the tip position of the next tooth (k^{th}).

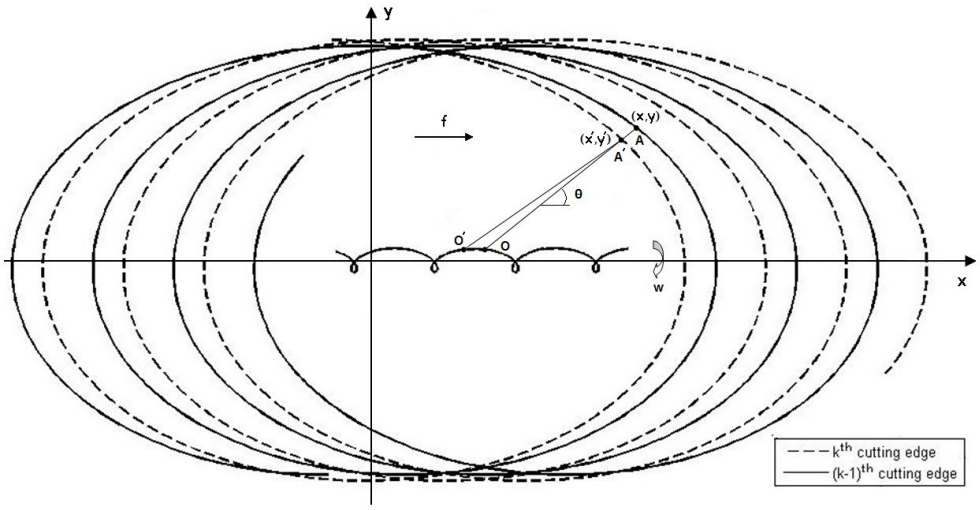

Figure 3.3. Trajectory of k^{th} and $(k-1)^{th}$ teeth.

The x, y coordinates of the trajectory of k^{th} edge can be given by

$$\begin{aligned} x_k &= s_t t + R\sin\left(wt - \frac{2\pi k}{K}\right) + R_0\sin\left(wt + \gamma_0\right) \\ y_k &= R\cos\left(wt - \frac{2\pi k}{K}\right) + R_0\cos\left(wt + \gamma_0\right) \end{aligned} \tag{11}$$

where s_t is the feed rate (mm/s), R is the radius of the tool (mm), w is the spindle angular velocity (rad/s), t is the time (s), k is the tooth number, K is the number of teeth, R_0 is the run-out magnitude (mm), and γ_0 is the run-out angle (rad). Eqs. (11) can be rewritten as:

$$y_k = \frac{x_k - s_t t - R\sin\left(wt + \gamma\right)}{\tan\left(wt - \frac{2\pi k}{K}\right)} + R_0\cos\left(wt + \gamma_0\right) \tag{12}$$

The x, y coordinates of (k-1)th edge trajectory can be found from Eqs. (11) by replacing k with (k-1) and t with t'.

$$\begin{aligned} x_{k-1} &= s_t \mathrm{t}' + R\sin\left(w\mathrm{t}' - \frac{2\pi(k-1)}{K}\right) + R_0\sin(w\mathrm{t}' + \gamma_0) \\ y_{k-1} &= R\cos\left(w\mathrm{t}' - \frac{2\pi(k-1)}{K}\right) + R_0\cos(w\mathrm{t}' + \gamma_0) \end{aligned} \tag{13}$$

To determine the time t', Eq. (13) is subsituted into Eq. (12) and the following equation is obtained:

$$\begin{aligned} F(\mathrm{t}') = {} & R\tan\left(wt - \frac{2\pi k}{K}\right)\cos\left(w\mathrm{t}' - \frac{2\pi(k-1)}{K}\right) + R_0\tan\left(wt - \frac{2\pi k}{K}\right)\cos(w\mathrm{t}' + \gamma_0) \\ & - R_0\tan\left(wt - \frac{2\pi k}{K}\right)\cos(wt + \gamma_0) - s_t\mathrm{t}' + s_t\mathrm{t} - R\sin\left(w\mathrm{t}' - \frac{2\pi(k-1)}{K}\right) - R_0\sin(w\mathrm{t}' + \gamma_0) \\ & + R_0\sin(wt + \gamma_0) = 0 \end{aligned} \tag{14}$$

To solve non-linear Eq. (14) with respect to time t', an initial guess must be assumed. Considering the angular velocity (w), the angle between the successive teeth, 2π/K rad takes 2π/(wK) s and the initial guess can then be taken as:

$$\mathrm{t}'_{\mathrm{i}} = \mathrm{t} - \frac{2\pi}{wK} \tag{15}$$

From iterative Newton-Raphson method, the following equation the time t' can be written:

$$\mathrm{t}'_{\mathrm{i+1}} = \mathrm{t}'_{\mathrm{i}} - \frac{F(\mathrm{t}'_{\mathrm{i}})}{F'(\mathrm{t}'_{\mathrm{i}})} \tag{16}$$

where the derivative of the F(t') function can be found by:

$$\begin{aligned} F(\mathrm{t}') = -w[& R\tan\left(wt - \frac{2\pi k}{K}\right)\sin\left(w\mathrm{t}' - \frac{2\pi(k-1)}{K}\right) + R_0\tan\left(wt - \frac{2\pi k}{K}\right)\sin(w\mathrm{t}' + \gamma_0) + \\ & R\cos\left(w\mathrm{t}' - \frac{2\pi(k-1)}{K}\right) + R_0\cos(w\mathrm{t}' + \gamma_0) - s_t] = 0 \end{aligned} \tag{17}$$

Considering the detailed geometry of our milling model, as shown in below Figure 3.4, the uncut chip thickness (h) formula can be developed as follows:

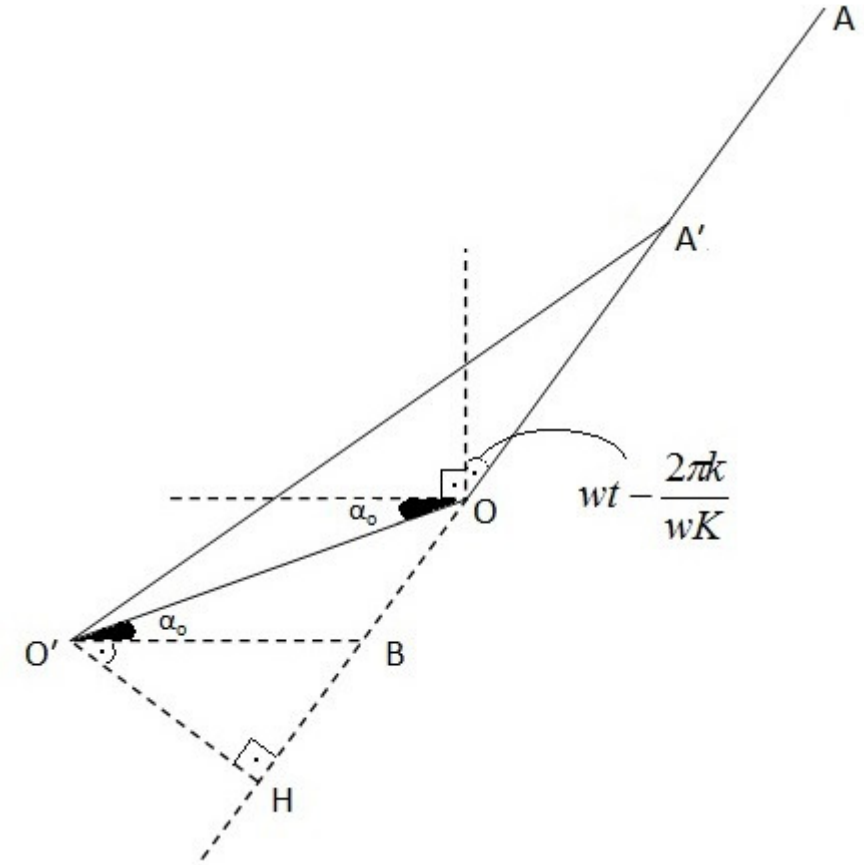

Figure 3.4: Modeling the geometry of chip formation by considering successive tool trajectories of k^{th} and $(k-1)^{th}$ teeth. O' and O refer to the tool center of $(k-1)^{th}$ and k^{th} teeth, respectively.

From the figure; $|A'O'| = |AO| = R$, $|OO'| = L$. Considering the k^{th} tool center, point O:

$$\alpha_0 + wt - \frac{2\pi k}{K} + m(O'\hat{O}H) = \frac{\pi}{2} \tag{18}$$

Considering the right triangle of $\overset{\Delta}{O'OH}$:

$$m(O'\hat{O}H) + \alpha_0 + m(B\hat{O}'H) = \frac{\pi}{2} \tag{19}$$

From equations 18 and 19, one can write:

$$m(B\hat{O}'H) = wt - \frac{2\pi k}{K}$$

The chip load, h (=$|AA'|$) can be written by:
$|AA'| = |AH| - |A'H| = |AO| + |OH| - |A'H|$
which leads to Eq. (20):

$$h = R + L\sin\left(wt - \frac{2\pi k}{K} + \alpha_0\right) - \sqrt{R^2 - L^2\cos^2\left(wt - \frac{2\pi k}{K} + \alpha_0\right)} \qquad (20)$$

where the distance, L and the angle, α_0 can be calculated as:

$$L = \sqrt{(x_o - x_{o'})^2 + (y_o - y_{o'})^2} \qquad \alpha_0 = \arctan\left(\frac{y_o - y_{o'}}{x_o - x_{o'}}\right) \qquad (21)$$

The coordinates of successive tool center positions are:

$$\begin{aligned} x_o &= s_t t + R_0\sin(wt + \gamma_0) & x_{o'} &= s_t t' + R_0\sin(wt' + \gamma_0) \\ y_o &= R_0\cos(wt + \gamma_0) & y_{o'} &= R_0\cos(wt' + \gamma_0) \end{aligned} \qquad (22)$$

The trochoidal tool path and run-out inclusions make the uncut chip thickness variation as shown in Figures 3.5 and 3.6, which are plotted at two feed rates (2.5 μm and 10 μm feed/tooth), spindle speed of 25,000 rpm and run-out angle of 45°. The effect of run-out length on uncut chip thickness can be compared by these figures.

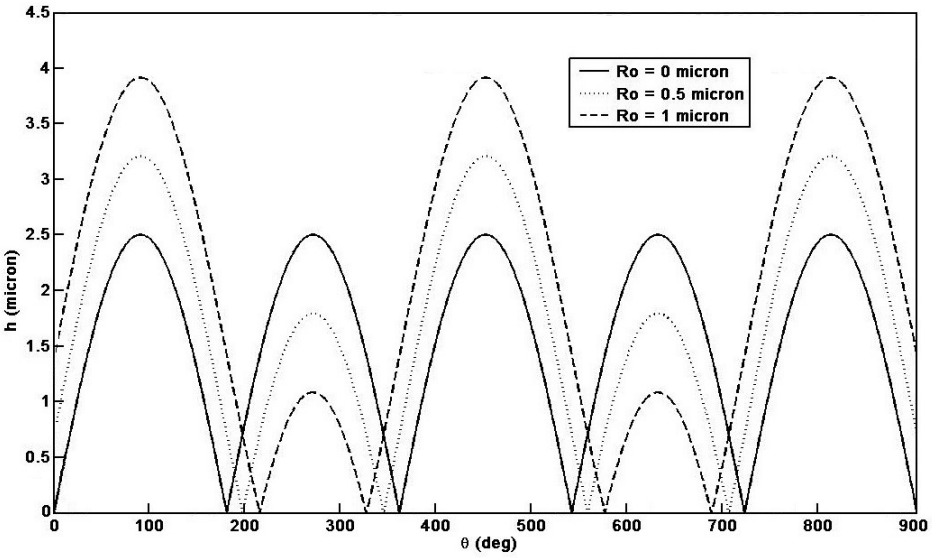

Figure 3.5: Uncut chip thickness variation for various run-out length at 2.5 μm feed/tooth and 45° run-out angle.

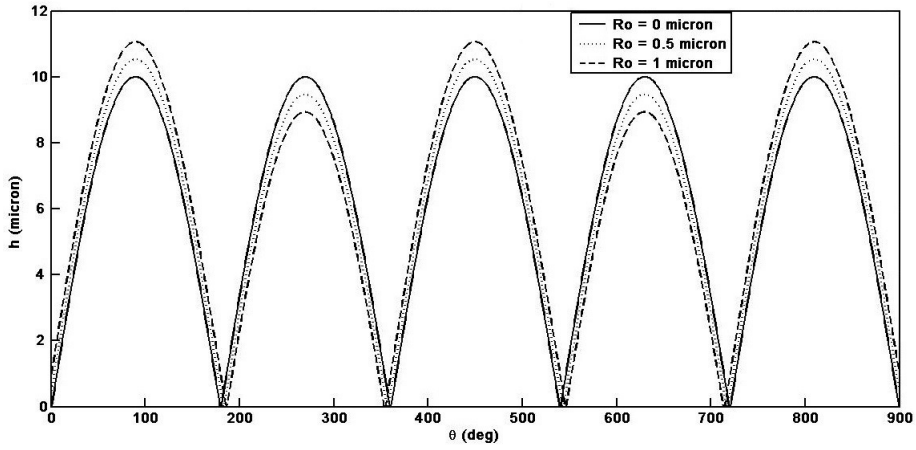

Figure 3.6: Uncut chip thickness variation for various run-out length at 10 μm feed/tooth and 45° run-out angle.

By increasing R_0, it can be observed that chip load increases for tooth 1 but decreases for tooth 2. Therefore tooth 1 is predicted to experience higher cutting forces due to larger chip load on the cutter.

Figure 3.7 can be observed for run-out length of 0.5 μm at 2.5 μm feed/tooth. With only run-out length, the uncut chip thickness varies as expected, i.e. the 1st tooth removes fewer chips than the 2nd tooth. For the run-out angle of 45°, the chip

load of the 1st tooth decrease while of the 2nd tooth increase. For 60°, the 1st tooth has far more chip load than the 2nd tooth.

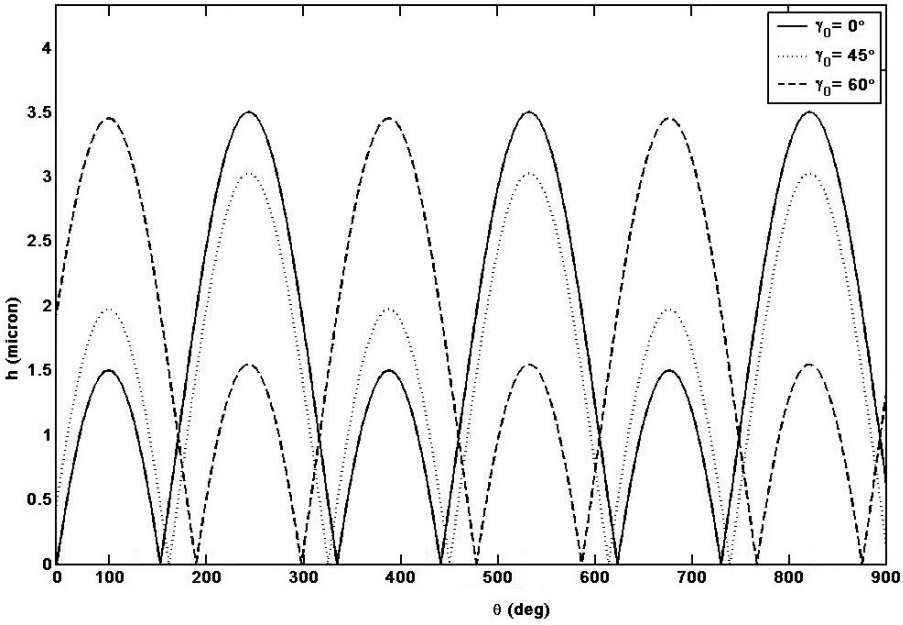

Figure 3.7: Uncut chip thickness variation for various run-out angle at 2.5 μm feed/tooth and 0.5 μm run-out length.

From tool runout modeling, it can be seen that chip thickness varies as a nonlinear function of runout distance and angle. The runout distance and angle can be measured in static conditions but in dynamic milling conditions runout values may be different due to milling forces acting on the tool and bending of the slender micro end mills.

3.4 Experimental Setup

In this chapter, the milling experiments were performed on the three axis milling machine (DMG HSC 55, Figure 3.8) equipped with a high speed Nakanishi spindle (HES510-HSKA63, Figure 3.9) with maximum spindle speed of 50,000 rpm, power of 350 W and a torque of 0.9 Nm . It has X, Y, and Z range of 450, 600, 400 mm, respectively.

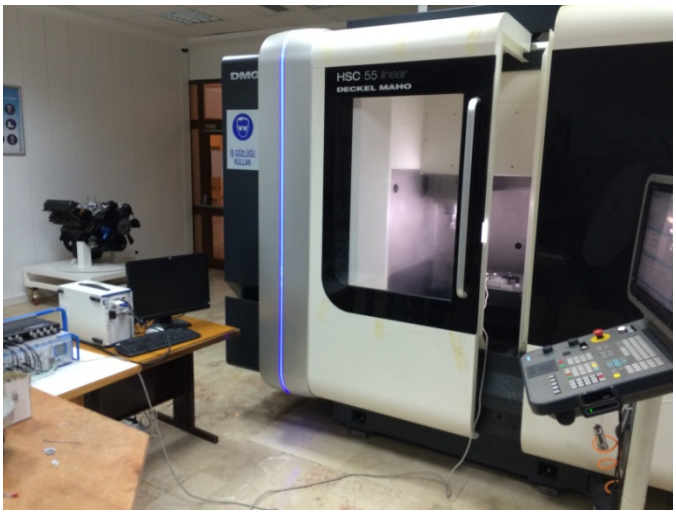

Figure 3.8: DMG HSC 55 milling machine, used for micro milling tests.

Figure 3.9: Nakanishi HES 510 spindle attached to the machine.

A 50 mm diameter Ti circular disc is used as a workpiece. Full slots are milled on the face of the disc. For these slots, an entrance channel of 0.4 mm depth and 2 mm width was machined. The reason behind these slots is to decrease the impact on the end mill during entry.

Flat micro end mills of 0.4 mm and 0.6 mm diameter (NS Tool Co., 2 teeth, 30° helix angle) are employed in micro machining tests. Figure 3.10 shows the

scanning electron microscope images of the micro end mills for 0.4 and 0.6 mm diameter. Cutting tool edge radius for this tool is measured to be around 2-3 µm.

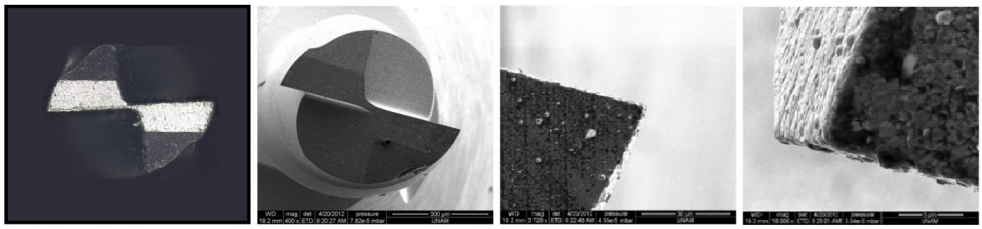

Figure 3.10: SEM images of flat micro end mills of 0.4 mm (a) and 0.6 mm

Two experiment sets was performed. Cutting tools with 0.4 mm and 0.6 mm diameter were evaluated by the model with run-out inclusion that was described in Section 3.3. The experimental conditions used are shown in Table 3.1. Spindle speeds are selected by considering the vibrational characteristics of the mini dynamometer and the milling machine. It can be seen that at the lowest feed rate, the feed per tooth is less than the edge radius of the cutting tool.

Table 3.1: Experimental Milling Conditions.

Tool Diameter (mm)	**Spindle Speed (rpm)**	**Cutting Speed (m/min)**	**Depth of Cut (µm)**	**Feed Rate (µm/tooth)**
0.4	26,000	32.7	76	1.5
			77	2
			76	3
			76	4
			79	6
			79	10
0.6	17,000	32.0	119	2
			120	4
			120	6
			121	8
			122	10

Each milling test was performed on fresh cutting tool so that the effect of wear on the forces can be eliminated.

Run-out Measurements of the Spindle

Defined as the inaccuracy of rotating mechanical system, the run-out of the cutting tool tip can be considered as a combination of the run-outs of the cutting tool and the spindle. This combined value is called as the tool run-out. Two parameters can be extracted from run-out measurements, which can be named as the radial and angular run-out. To specify the magnitude and the effect of each, run-out should be measured at different places and the results should be evaluated. By the dial indicator, the run-out can be measured statically. For this purpose, the probe of the indicator is touched to the shank of the cutting tool. Then the deviations are measured by turning the spindle in clockwise direction by 180°. The maximum deviation with respect to the reference can be specified as the tool run-out. In this study, the run-out of the Nakanishi HES 510 spindle was measured by Mahr Milimar C1208 Compact Amplifier. The measurement was performed after the spindle is mounted on the DMG vertical milling centre. A 4 mm diameter WC rod is mounted on the spindle with a collet type tool holder. The probe of the instrument was touched into the tip at one point and that point is accepted as a reference point. Then the tool tip was rotated manually by 60° angular increments (to encompass one full rotation) and at each increment the deviation from the reference value is recorded. This process was repeated at various axial levels (z axis) of the rod and the measurements were performed. Figure 3.11 illustrates the measurement setup for run-out measurement. The measured deviations from the reference were less than 1 μm.

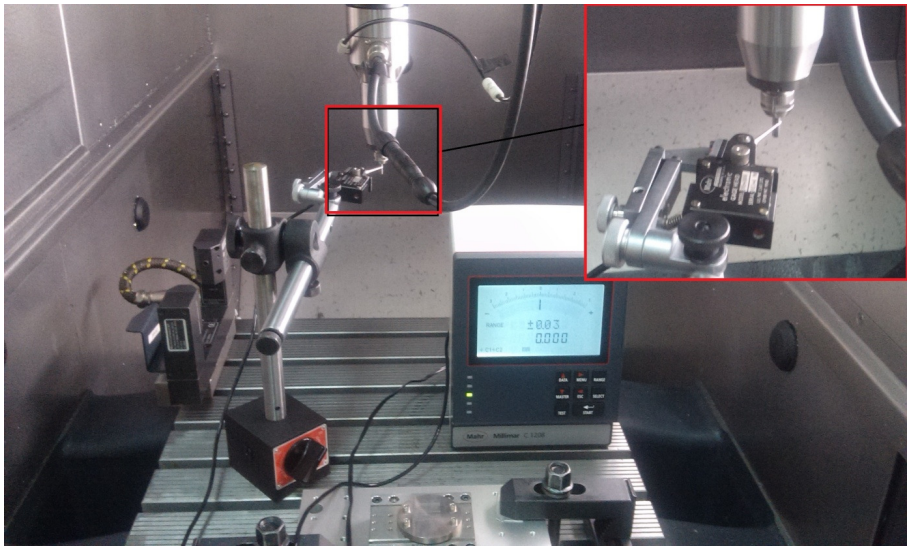

Figure 3.11: Run–out measurement setup.

3.5 Micro Milling Tests (Run-Out Included)

3.5.1 Experiments with 0.6 mm diameter cutting tool

Average forces taken through the experiments are plotted for this cutting tool at 17,000 rpm spindle speed. Figure 3.12 shows the average force data and Table 3.2 shows the cutting and edge force coefficients that were calculated from this data.

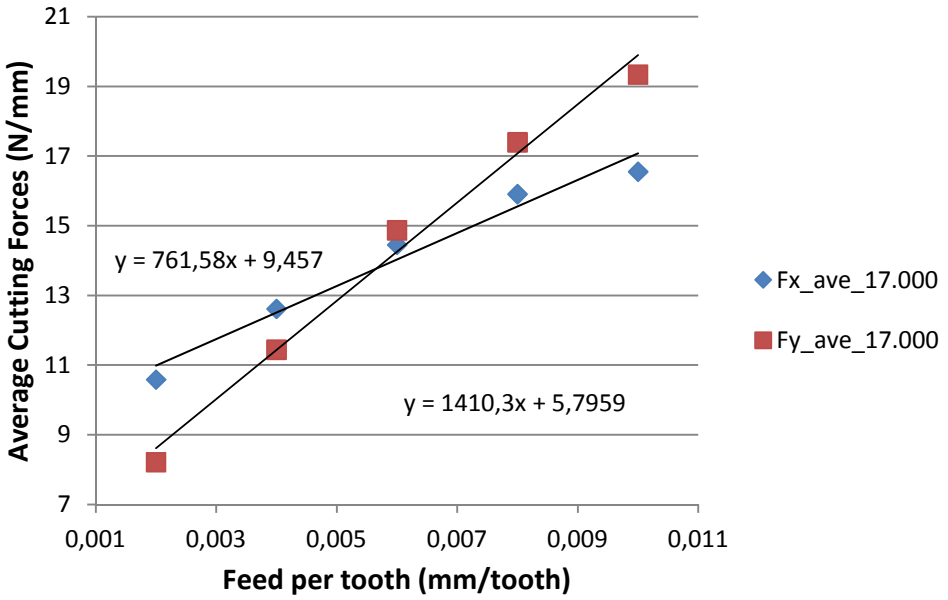

Figure 3.12: 17,000 rpm, 0.12 mm depth of cut, 0.6 mm diameter, Ti6Al4V.

Table 3.2: Calculated cutting and edge force coefficients for 0.6 mm tool at 17,000 rpm spindle speeds.

k_{te} (N/mm²)	k_t (N/mm)	k_{ne} (N/mm²)	k_n (N/mm)
9.1042	2820.4	14.855	1523.2

The instantaneous milling forces are calculated with the assumption that the spindle has 1 μm run-out, as measured in the previous section. Figure 3.13 shows the simulated and experimental force results. Table 3.3 gives the errors in the peak instantaneous force values of the model.

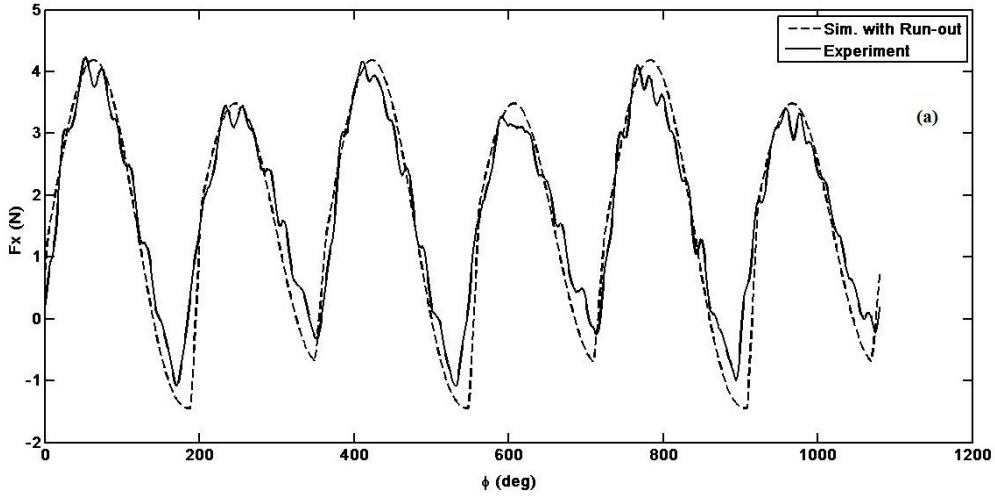

(a) F_x

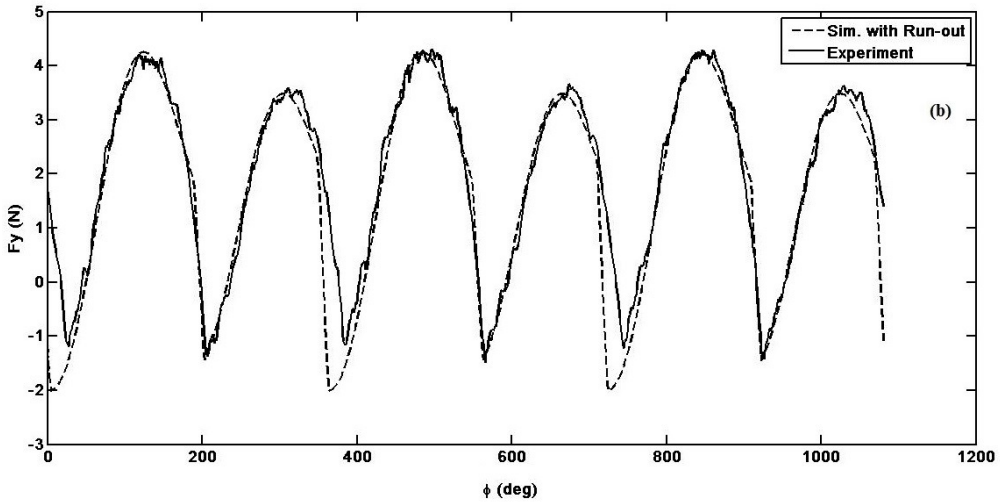

(b) F_y

Figure 3.13: Instantaneous milling force values measured and predicted for 17,000 rpm, 0.6 mm diameter cutting tool on Ti6Al4V workpiece with 0.120 mm depth of cut and 6 μm feed/tooth conditions; a)F_x and b)F_y.

Table 3.3: Errors in the peak instantaneous force values for 0.6 mm diameter tool at 17,000 rpm speed for the Nakanishi spindle with 6 µm feed/tooth.

	1st tooth				2nd tooth			
	max F_x (N)		max F_y (N)		max F_x (N)		max F_y (N)	
	Exp.	Simu.	Exp.	Simu.	Exp.	Simu.	Exp.	Simu.
	4.205	4.188	4.286	4.277	3.267	3.245	3.519	3.218
Error,%	-0.40		-0.21		-0.67		-8.55	

It can be seen from Figure 3.13 and Table 3.3 that the micro scale model with realistic chip thickness values together with runout model can predict the instantaneous cutting forces quite well.

3.5.2 Experiments with 0.4 mm diameter cutting tool

Average forces taken through the experiments are plotted for this cutting tool at 26,000 rpm spindle speed, with line-fits as shown in Figure 3.14. Table 3.4 shows the cutting and edge force coefficients of linear fit assumption.

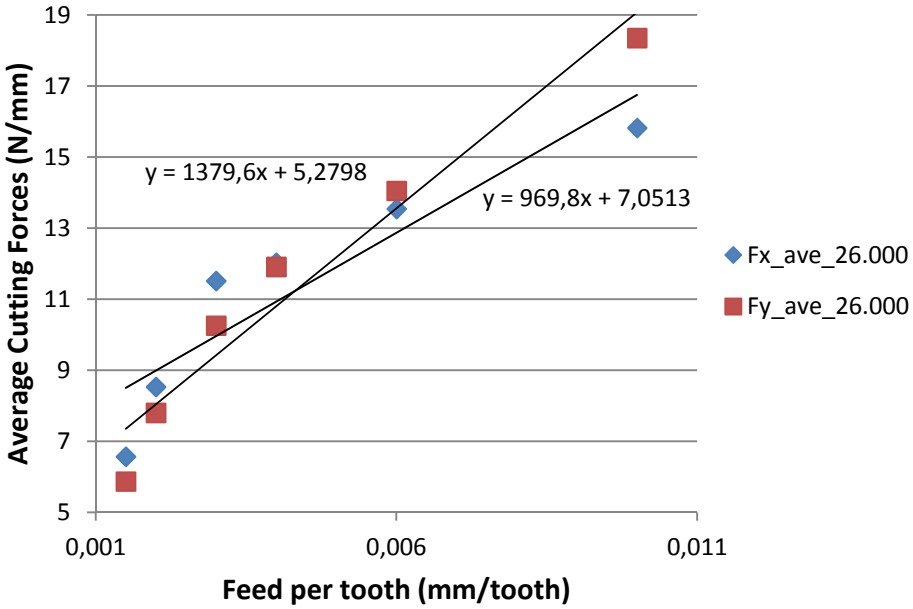

Figure 3.14: Linear fit with test results for 26,000 rpm, 0.08 mm depth of cut, 0.4 mm diameter, Ti6Al4V.

Table 3.4: Calculated cutting and edge force coefficients for 0.4 mm tool at 26,000 rpm spindle speeds.

k_{te} (N/mm²)	k_t (N/mm)	k_{ne} (N/mm²)	k_n (N/mm)
8.29	2759	11.08	1940

When the coefficients obtained for 0.6 and 0.4 mm diameter tools are compared, it can be seen that the cutting and edge force coefficients in tangential direction are quite similar. Since cutting force coefficients in tangential direction are related to material being cut, this is an expected result. When the cutting and edge force coefficients in radial direction are compared, the 0.4 mm diameter tool yielded larger cutting force coefficients. Another observation from Figure 3.14 is that, the linear fit may not be adequate to represent the average cutting forces between 1.5 µm and 6 µm feed/tooth values. The linear fit especially deviates from the experimental results at low and high feed values. Figure 3.15 shows the same data with polynomial fit. It can be seen that a better fit can be obtained. However, the cutting and edge force coefficient calculations must be derived for a polynomial fit.

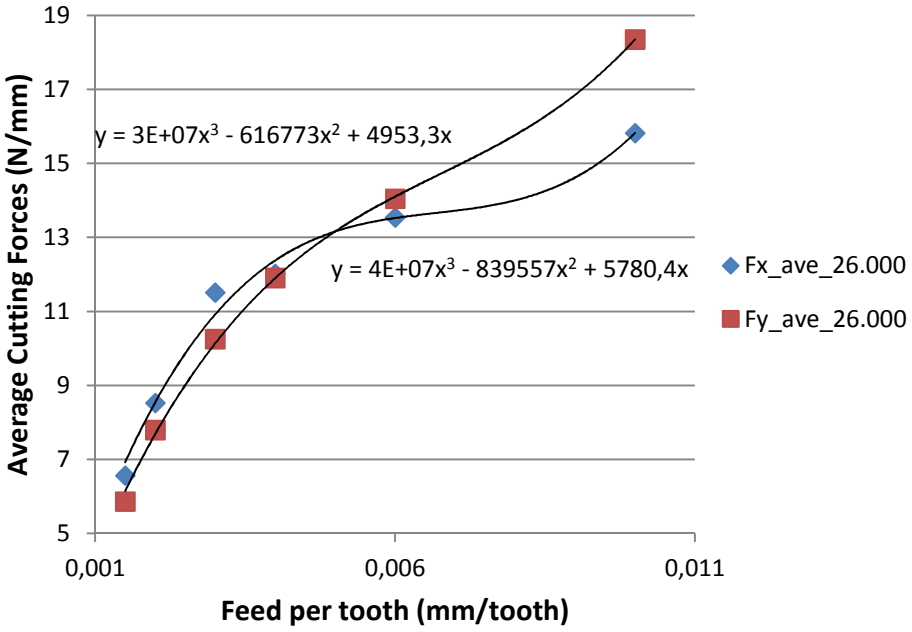

Figure 3.15: Polynomial fit with test results for 26,000 rpm, 0.08 mm depth of cut, 0.4 mm diameter, Ti6Al4V.

3.5.3 Calculation of Cutting Force Coefficients for Polynomial Fit

In this section, for the milling experiments with 0.4 mm diameter tool, a polynomial representation has been proposed for the cutting forces. First the necessary equations are derived, then linear and polynomial fit assumptions are compared. Let us assume that, a third order polynomial equation can be used to represent the trend of average forces as shown in Figure 3.15. Eq. (23) shows the elemental forces in tangential and radial directions.

$$\begin{aligned} dF_{t_j} &= (k_{t0} + k_{t1} h_j + k_{t2} h_j^{\,2} + k_{t3} h_j^{\,3}) dz \\ dF_{n_j} &= (k_{n0} + k_{n1} h_j + k_{n2} h_j^{\,2} + k_{n3} h_j^{\,3}) dz \end{aligned} \tag{23}$$

The forces in tangential and radial directions can be transformed into x and y coordinates as shown in Eq. (24).

$$\begin{aligned} dF_{x_j} &= \begin{bmatrix} k_{t0}\cos\phi_j + k_{n0}\sin\phi_j + (k_{t1}\cos\phi_j + k_{n1}\sin\phi_j) h_j + \\ (k_{t2}\cos\phi_j + k_{n2}\sin\phi_j) h_j^{\,2} + (k_{t3}\cos\phi_j + k_{n3}\sin\phi_j) h_j^{\,3} \end{bmatrix} dz \\ dF_{y_j} &= \begin{bmatrix} k_{t0}\sin\phi_j - k_{n0}\cos\phi_j + (k_{t1}\sin\phi_j - k_{n1}\cos\phi_j) h_j + \\ (k_{t2}\sin\phi_j - k_{n2}1\cos\phi_j) h_j^{\,2} + (k_{t3}\sin\phi_j - k_{n3}1\cos\phi_j) h_j^{\,3} \end{bmatrix} dz \end{aligned} \tag{24}$$

The average forces can be calculated by taking the integrals of Eq. (24):

$$\int dF_{x_j} = \frac{R}{\tan i} \begin{bmatrix} -k_{t0}\sin\phi_j + k_{r0}\cos\phi_j + \frac{s_t}{4}\left[k_{t1}\cos 2\phi_j + k_{n1}(-2\phi_j + \sin 2\phi_j)\right] + \\ \frac{s_t^{\,2}}{12}\left[-4k_{t2}\sin^3\phi_j - k_{n2}(\cos 3\phi_j - 9\cos\phi_j)\right] + \\ \frac{s_t^{\,3}}{32}\left[-8k_{t3}\sin^4\phi_j - k_{n3}(12\phi_j - 8\sin 2\phi_j + \sin 4\phi_j)\right] \end{bmatrix}_{z_{j,1}(\phi)}^{z_{j,2}(\phi)} \tag{25}$$

$$\int dF_{y_j} = \frac{R}{\tan i} \begin{bmatrix} k_{t0}\cos\phi_j + k_{r0}\sin\phi_j + \frac{s_t}{4}\left[k_{t1}(-2\phi_j + \sin 2\phi_j) - k_{n1}\cos 2\phi_j\right] + \\ \frac{s_t^{\,2}}{12}\left[-k_{t2}(\cos 3\phi_j - 9\cos\phi_j) + 4k_{n2}\sin^3\phi_j\right] + \\ \frac{s_t^{\,3}}{32}\left[-k_{t3}(12\phi_j - 8\sin 2\phi_j + \sin 4\phi_j) + 8k_{n3}\sin^4\phi_j\right] \end{bmatrix}_{z_{j,1}(\phi)}^{z_{j,2}(\phi)}$$

By taking the number of tooth on the cutter into account, the average forces can be calculated as Eqs. (26).

$$\overline{F_x} = \frac{aN}{2\pi}\left[\begin{array}{l} k_{t0}\sin\phi_j - k_{n0}\cos\phi_j + \frac{s_t}{4}\left[-k_{t1}\cos 2\phi_j + k_{n1}(2\phi_j - \sin 2\phi_j)\right] + \\ \frac{s_t^2}{12}\left[4k_{t2}\sin^3\phi_j + k_{n2}(\cos 3\phi_j - 9\cos\phi_j)\right] + \\ \frac{s_t^3}{32}\left[8k_{t3}\sin^4\phi_j + k_{n3}(12\phi_j - 8\sin 2\phi_j + \sin 4\phi_j)\right] \end{array}\right]_{\phi_{st}}^{\phi_{ex}}$$

$$\overline{F_y} = \frac{aN}{2\pi}\left[\begin{array}{l} -k_{t0}\cos\phi_j - k_{n0}\sin\phi_j + \frac{s_t}{4}\left[k_{t1}(2\phi_j - \sin 2\phi_j) + k_{n1}\cos 2\phi_j\right] + \\ \frac{s_t^2}{12}\left[k_{t2}(\cos 3\phi_j - 9\cos\phi_j) - 4k_{n2}\sin^3\phi_j\right] + \\ \frac{s_t^3}{32}\left[k_{t3}(12\phi_j - 8\sin 2\phi_j + \sin 4\phi_j) - 8k_{n3}\sin^4\phi_j\right] \end{array}\right]_{\phi_{st}}^{\phi_{ex}} \quad (26)$$

By defining the following set of equations,

$$A = \frac{aN}{2\pi}\left[\cos\phi\right]_{\phi_{st}}^{\phi_{ex}} \qquad B = \frac{aN}{2\pi}\left[\sin\phi\right]_{\phi_{st}}^{\phi_{ex}} \qquad C = \frac{aN}{2\pi}\left[2\phi - \sin 2\phi\right]_{\phi_{st}}^{\phi_{ex}}$$

$$D = \frac{aN}{2\pi}\left[\cos 2\phi\right]_{\phi_{st}}^{\phi_{ex}} \qquad E = \frac{aN}{2\pi}\left[\cos 3\phi - 9\cos\phi\right]_{\phi_{st}}^{\phi_{ex}} \qquad F = \frac{aN}{2\pi}\left[\sin^3\phi\right]_{\phi_{st}}^{\phi_{ex}}$$

$$G = \frac{aN}{2\pi}\left[12\phi - 8\sin 2\phi + \sin 4\phi\right]_{\phi_{st}}^{\phi_{ex}} \qquad H = \frac{aN}{2\pi}\left[\sin^4\phi\right]_{\phi_{st}}^{\phi_{ex}} \quad (27)$$

By these coefficients, the average forces can be represented as follows:

$$\begin{aligned} \overline{F_x} &= k_{t0}B - k_{n0}A + \frac{s_t}{4}\left(-k_{t1}D + k_{n1}C\right) + \frac{s_t^2}{12}\left(4k_{t2}F + k_{n2}E\right) + \frac{s_t^3}{32}\left(8k_{t3}H + k_{n3}G\right) \\ \overline{F_y} &= -k_{t0}A - k_{n0}B + \frac{s_t}{4}\left(k_{t1}C + k_{n1}D\right) + \frac{s_t^2}{12}\left(k_{t2}E - 4k_{n2}F\right) + \frac{s_t^3}{32}\left(k_{t3}G - 8k_{n3}H\right) \end{aligned} \quad (28)$$

The experimental average cutting forces in X and Y direction can be represented with as shown in Figure 3.15.

$$\overline{F_x} = \overline{F_{x0}} + \overline{F_{x1}}s_t + \overline{F_{x2}}s_t^2 + \overline{F_{x3}}s_t^3 \qquad \overline{F_y} = \overline{F_{y0}} + \overline{F_{y1}}s_t + \overline{F_{y2}}s_t^2 + \overline{F_{y3}}s_t^3 \quad (29)$$

By equating the respective force values of Eqs. (28) and (29) in x and y directions k_{t0}, k_{t1}, k_{t2}, k_{t3}, k_{r0}, k_{r1}, k_{r2} and k_{r3} can be found as follows:

$$k_{t0} = \frac{\overline{F_{x0}}B - \overline{F_{y0}}A}{A^2 + B^2} \qquad k_{t1} = 4\frac{\overline{F_{y1}}C - \overline{F_{x1}}D}{C^2 + D^2} \qquad k_{t2} = 12\frac{\overline{F_{y2}}E + 4\overline{F_{x2}}F}{E^2 + 16F^2}$$

$$k_{t3} = 32\frac{\overline{F_{y3}}G + 8\overline{F_{x3}}H}{G^2 + 64H^2} \qquad k_{n0} = \frac{\overline{F_{y0}}B - \overline{F_{x0}}A}{B^2 + A^2} \qquad k_{n1} = 4\frac{\overline{F_{y1}}D + \overline{F_{x1}}C}{C^2 + D^2}$$

$$k_{n2} = 12\frac{\overline{F_{x2}}E - 4\overline{F_{y2}}F}{E^2 + 16F^2} \qquad k_{n3} = 32\frac{\overline{F_{x3}}G - 8\overline{F_{y3}}H}{G^2 + 64H^2} \tag{30}$$

Table 3.5 gives the cutting force coefficients depending on polynomial fit assumption.

Table 3.5: Calculated polynomial fit coefficients and cutting force coefficients for 0.4 mm tool at 26,000 rpm spindle speed.

Unit	**(N/mm)**	**(N/mm²)**	**(N/mm³)**	**(N/mm⁴)**
Polynom fit coefficients	$\overline{F_{x0}}$	$\overline{F_{x1}}$	$\overline{F_{x2}}$	$\overline{F_{x3}}$
	0	6099.2	-877467	$4\text{x}10^7$
	$\overline{F_{y0}}$	$\overline{F_{y1}}$	$\overline{F_{y2}}$	$\overline{F_{y3}}$
	0	4953.3	-616773	$3\text{x}10^7$
Cutting force coefficients	$\mathbf{k_{t0}}$	$\mathbf{k_{t1}}$	$\mathbf{k_{t2}}$	$\mathbf{k_{t3}}$
	0	9906.6	$-1.453237\text{x}10^6$	$8\text{x}10^7$
	$\mathbf{k_{n0}}$	$\mathbf{k_{n1}}$	$\mathbf{k_{n2}}$	$\mathbf{k_{n3}}$
	0	$12.2\text{x}10^4$	$-2.067483\text{x}10^6$	$1.067\text{x}10^8$

3.5.4 Comparison between linear and polynomial fits

By using cutting force coefficients, plots showing the instantaneous cutting forces can be drawn as shown in the below figure.

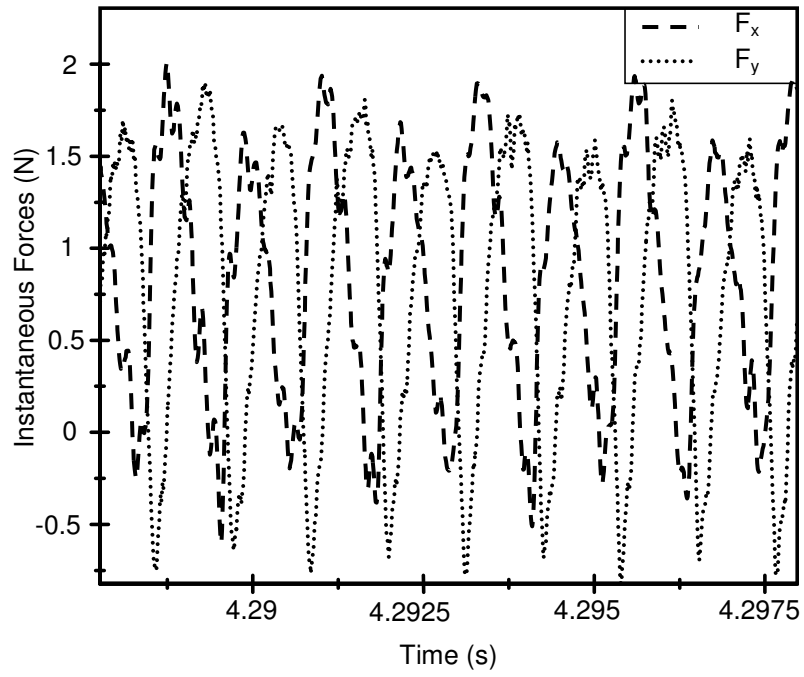
F_x
F_y
Instantaneous Forces (N)
2
1.5
1
0.5
0
-0.5
4.29
4.2925
4.295
4.2975
Time (s)

(a)

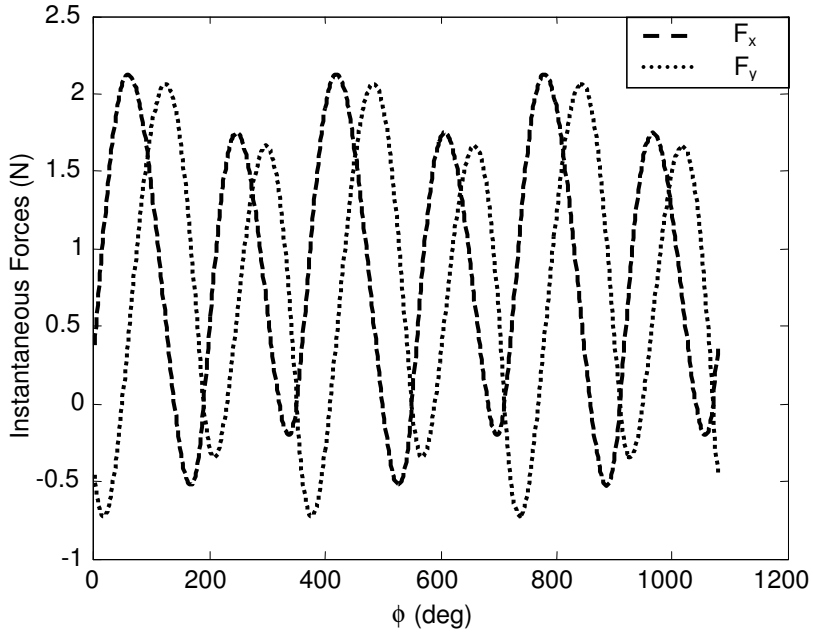
F_x
F_y
Instantaneous Forces (N)
2.5
2
1.5
1
0.5
0
-0.5
-1
0
200
400
600
800
1000
1200
ϕ (deg)

(b)

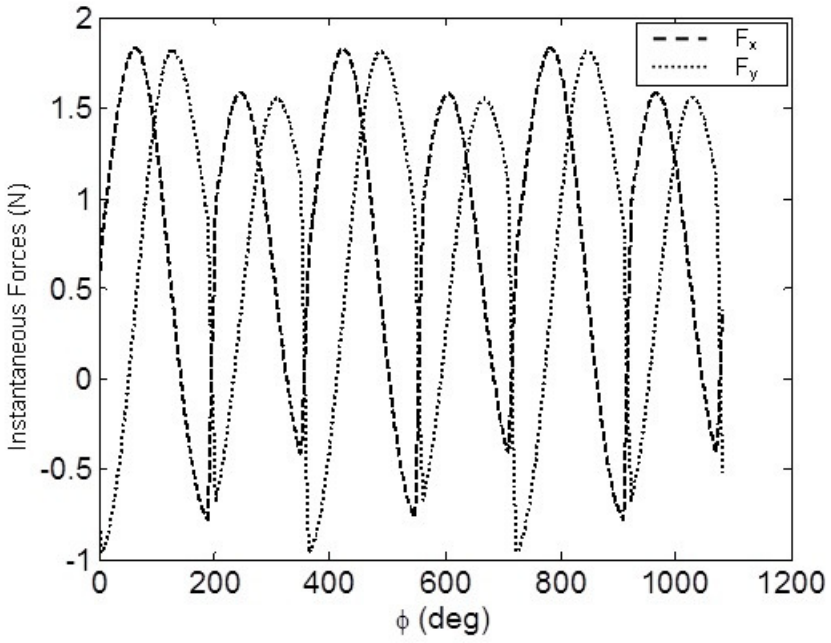

(c)

Figure 3.16: Instantaneous milling force values (Fx and Fy) for 26,000 rpm, 0.4 mm diameter cutting tool on Ti6Al4V workpiece with 0.076 mm depth of cut and 3 μm feed/tooth conditions. a) measured, b) predicted with polynomial, c) predicted with linear model.

From Figure 3.16 it can be seen that the polynomial fit assumption yields good results for cutting force calculations. In the predictions, runout values of 0.5 μm and 60 degrees were used.

Chapter 4

Investigation of Micro Milling Process Performed on Spindles with Large Runout

4.1 Overview And Aim

The effect of runout on micro milling forces has been studied in previous chapter. A special spindle with very low runout was used in experiments. In practice, micro milling is usually performed on spindles which are not designed for micro milling but general purpose. In this chapter, micro milling process when perfomed on spindles with large runout will be investigated. The applicability of the micro milling modeling derived in previous chapter will be studied.

4.2 Experimental Setup

Machining experiments were performed in micro machining center (Mikrotools DT-110) equipped with Precise SC 3062 spindle as shown in Figure 4.1.

(a)

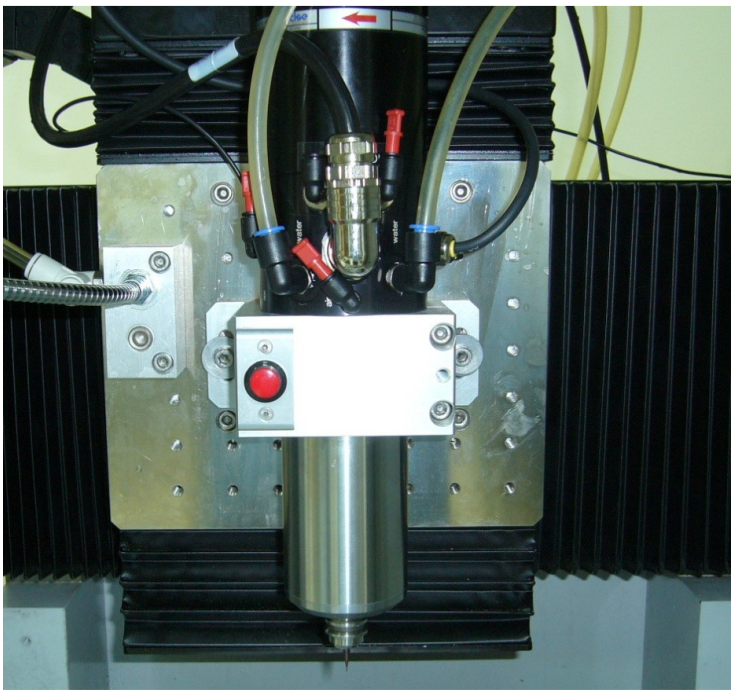

(b)

Figure 4.1 Test setup

Test setup including spindle, cutting tool, workpiece and force dynamometer can be seen in Figure 4.2.

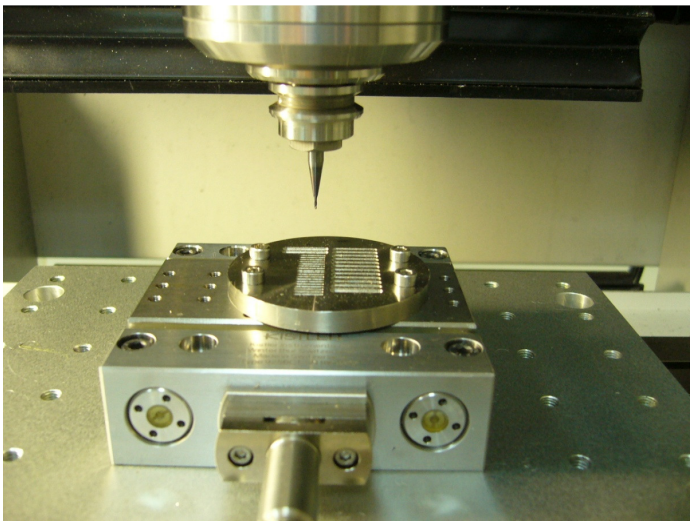

Figure 4.2: Micro milling test setup considered in this study.

The run-out of the Precise spindle is measured as 20-25 µm based on the measurement procedure described in Chapter 3. Figure 4.3 shows the runout on the spindle axis at two different heights.

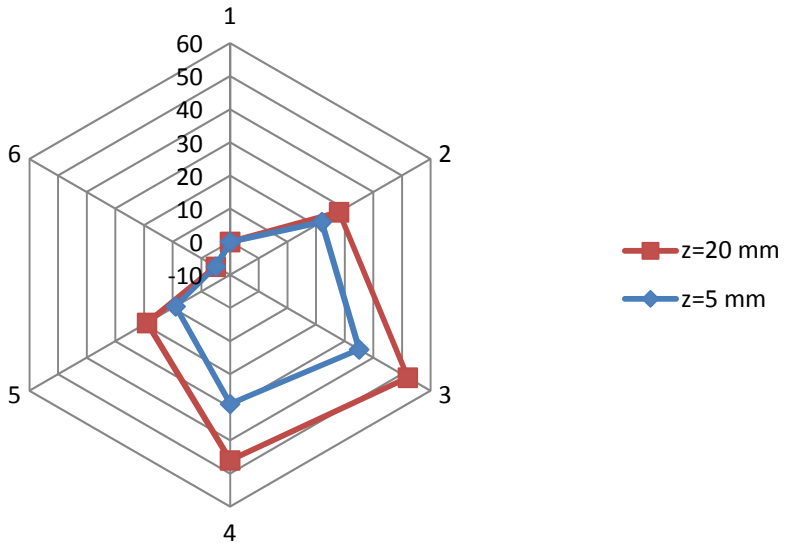

Figure 4.3. Static runout measurements on the tool body.

Full immersion experiments (slot milling) on Ti6Al7V are conducted using a 0.6 mm diameter tools on Precise spindle. For these slots, an entrance channel of 0.4 mm depth and 2 mm width was machined as before. In order to be able to compare the results obtained in two different spindles, the tool diameter is kept constant. Micro end mills from the same batch are used. It was observed that there is no significant variation in the dimension and geometry of the tools. Selected microtools has been used for slot milling under the same machining conditions using two different spindles. Overhang of the microtools are also adjusted to be the same in both group of tests to eliminate its effect on the cutting force measurements.

Only 17,000 rpm cutting speed for each cutting tool is experimented for four different feed rates. Table 4.1 shows the preliminary experimental conditions for both spindles used in this study.

Table 4.1: Experimental conditions for micro milling tests.

Tool Diameter (mm)	**Spindle Speed (rpm)**	**Depth of Cut (μm)**	**Feed Rate (μm/tooth)**
0.6	17,000	120	2-4-6-8

4.3 Micro Milling Tests

4.3.1 0.6 mm diameter tool on Precise Spindle

With 0.6 mm diameter tool on the Precise spindle the following results were obtained. The average forces and shown in Figure 4.4. Table 4.2 shows the cutting and edge force coefficients for the Precise spindle.

Table 4.2: Calculated cutting and edge force coefficients for 17,000 rpm for Precise spindle.

k_{te} (N/mm²)	k_t (N/mm)	k_{ne} (N/mm²)	k_n (N/mm)
4.1888	3391.6	3.6128	3539.2

The results given in Table 3.2 can be observed for the big difference in the cutting force and edge coefficients obtained in NSK spindle. Different run-outs of the spindle such as 1 and 20 μm affect the cutting conditions quite differently.

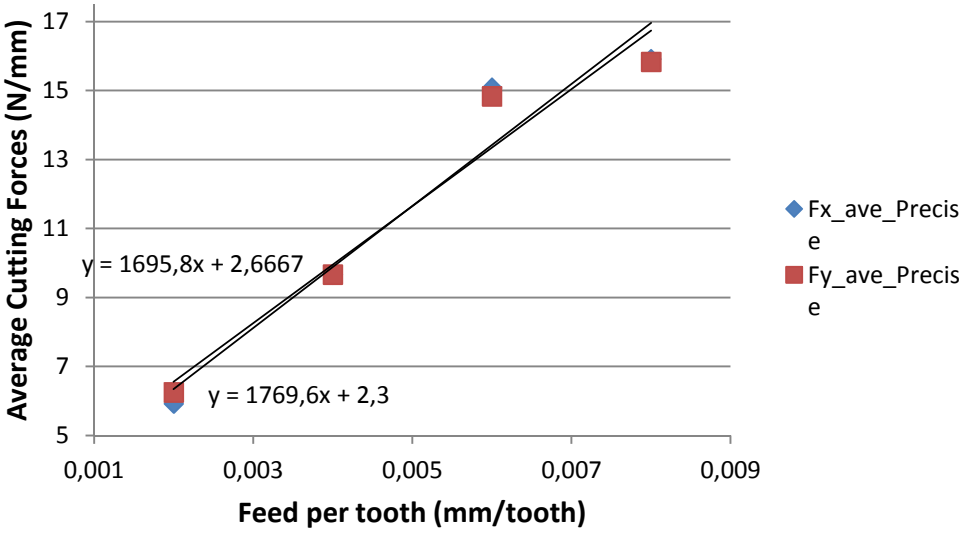

Figure 4.4: 17,000 rpm, 0.12 mm depth of cut, 0.6 mm diameter, Ti6Al4V, by Precise spindle.

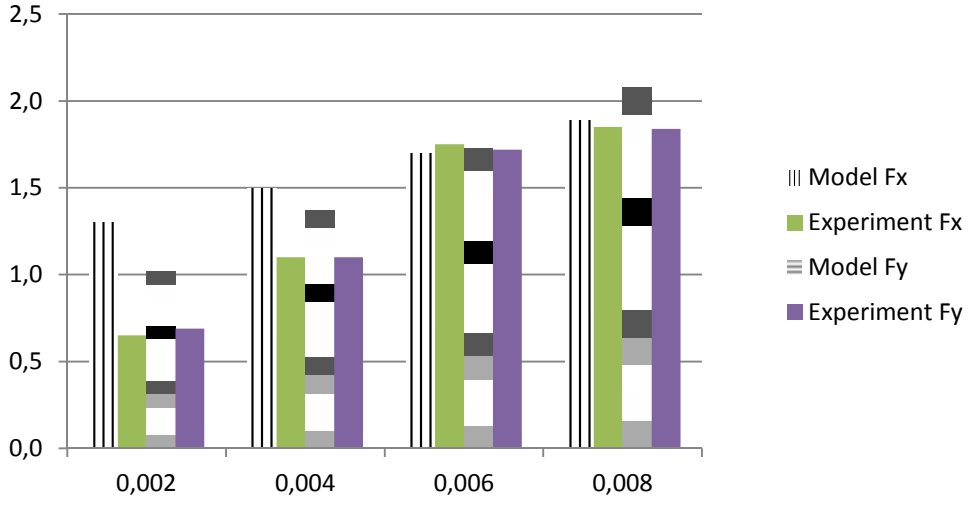

Figure 4.5: Average milling force values measured and predicted for 0.6 mm diameter cutting tool on Ti6Al4V workpiece with 17,000 rpm, 0.2 mm depth of cut and various feed/tooth conditions, by Precise spindle.

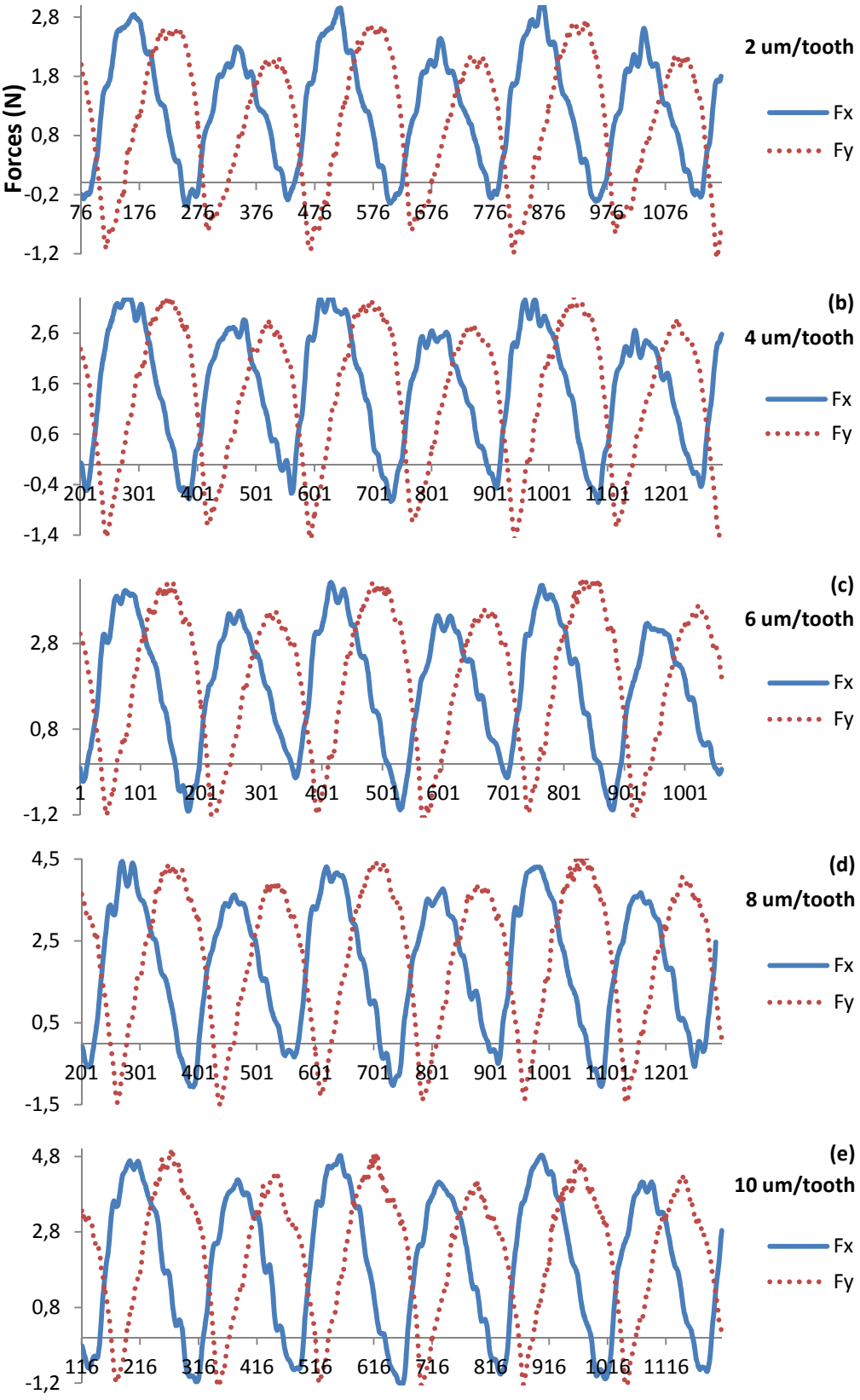
Forces (N)
2,8
1,8
0,8
-0,2
-1,2
76 176 276 376 476 576 676 776 876 976 1076
2 um/tooth
Fx
Fy
(b)
2,6
1,6
0,6
-0,4
-1,4
201 301 401 501 601 701 801 901 1001 1101 1201
4 um/tooth
Fx
Fy
(c)
2,8
0,8
-1,2
1 101 201 301 401 501 601 701 801 901 1001
6 um/tooth
Fx
Fy
4,5
2,5
0,5
-1,5
201 301 401 501 601 701 801 901 1001 1101 1201
(d)
8 um/tooth
Fx
Fy
4,8
2,8
0,8
-1,2
116 216 316 416 516 616 716 816 916 1016 1116
(e)
10 um/tooth
Fx
Fy

Figure 4.6: Instantaneous milling force values measured for Nakanishi (NSK) spindle with 17,000 rpm, 0.6 mm diameter cutting tool on Ti6Al4V workpiece with 0.12 mm depth of cut and various feed rate conditions.

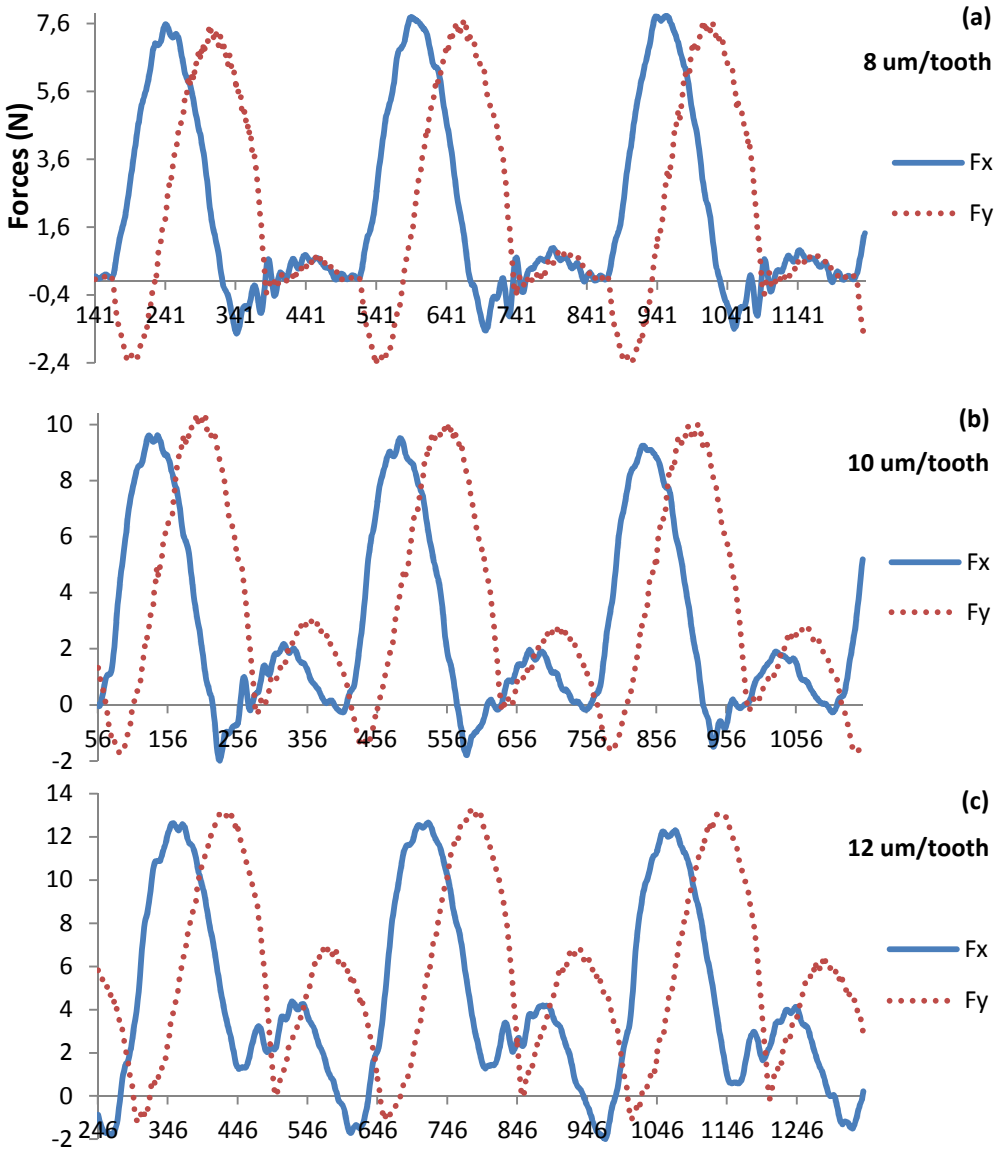

Figure 4.7: Instantaneous milling force values measured for Precise spindle with 17,000 rpm, 0.6 mm diameter cutting tool on Ti6Al4V workpiece with 0.12 mm depth of cut and various feed rate conditions.

From Figure 4.6, it can be seen that both teeth of the cutter is in contact with the workpiece during rotation of the cutting tool. The difference in the peak forces is low, indicating that the feed is larger than the runout value. As Precise spindle, for 8 μm feed per tooth case, no forces were observed on the second teeth. When feed per tooth is increased to 10 μm, the second tooth seems to start working. As feed per tooth is increased to 12 μm, peak force in the second tooth increased further. It seems like the statically measured runout value of 20 μm is not valid during actual micro milling process. Figure 4.8 shows that NSK spindle forces can be predicted very well with the cutting coefficients obtained in Table 3.2.

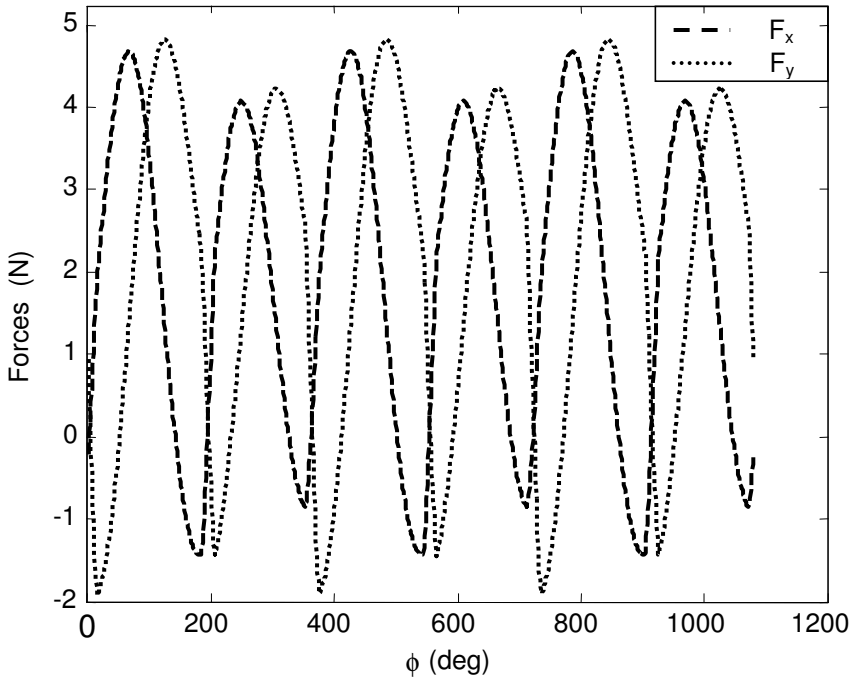

Figure 4.8. Predictions on 0.6 mm diameter tool with 8 μm feed per tooth on NSK spindle.

Cutting tools cannot be produced with a perfectly sharp cutting edge, which means that every cutting edge has some finite radius. During milling action, the cutting edge cannot take the chip out from the workpiece unless the uncut chip thickness is greater than some ratio of the edge radius. There is a specific value of minimum chip thickness, below which no chip is created during milling. Cutting edge ploughs the workpiece surface without creating any chips. Minimum chip

thickness effect influenced the ploughing force, which can be specified to be related with edge force coefficients. Compared to cutting force coefficients, edge force coefficients are very low (Table 2.2, 3.2, 3.4, 4.2). When the chip load / edge radius ratio is high, they have very little effect on the cutting forces. But when this ratio is low, they increase in magnitude and make the ploughing force have higher values than the cutting force. Ploughing force acts in the tertiary shear zone between workpiece and cutting tool. This zone comes out as the machined surface of the workpiece. Minimum chip thickness effect appears with dominant ploughing force.

In Figure 4.9 the instantaneous force predictions can be observed for the Precise spindle for various feed rates. The tool run-out was taken as 7.5 μm. Increasing effect of the ploughing force can be recognized along with decreasing feed rate values, which causes the cutting forces on the 2nd tooth to decline.

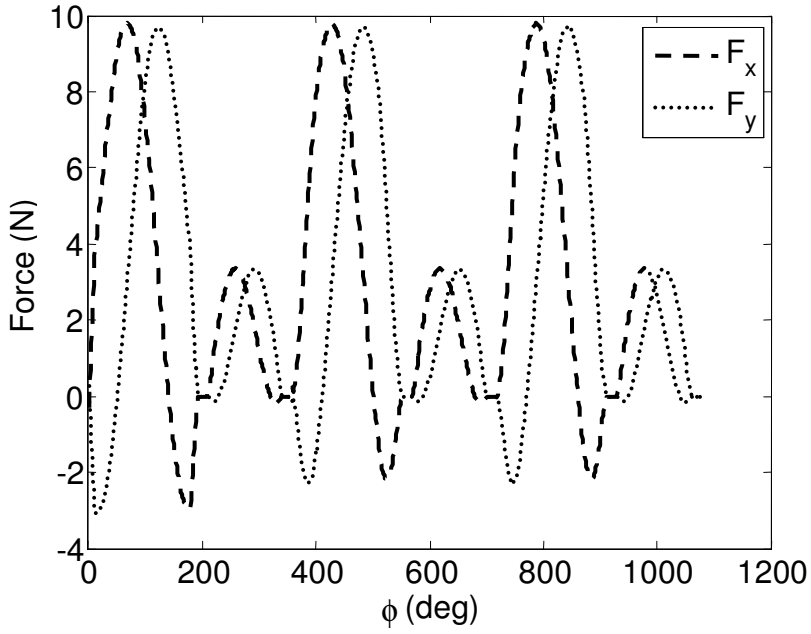

(a)

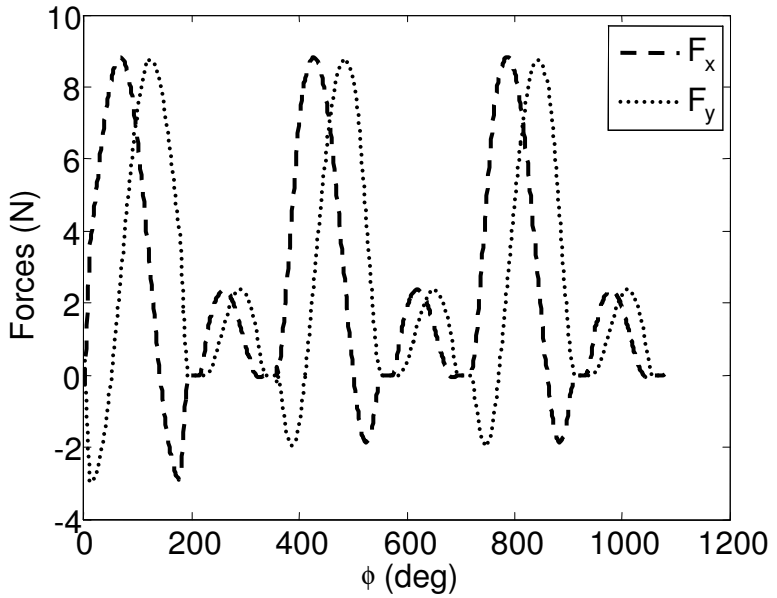

(b)

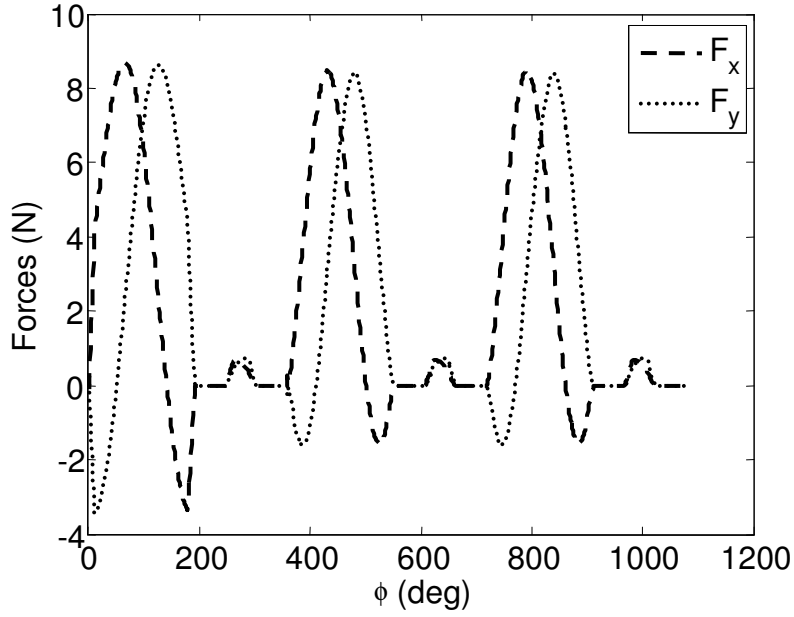

(c)

Figure 4.9. Predictions on 0.6 mm diameter tool with a) 12 μm feed per tooth on Precise spindle, b) 10 μm feed per tooth, c) 8 μm feed per tooth with 7.5 μm runout.

Figure 4.10 shows predicted and measured instantaneous force plots for Precise spindle with 2 µm/tooth feed rate. For such a low feed rate value comparable with the cutting edge radius, one of the teeth can not cut the workpiece. For the same feed rate with Nakanish spindle, both teeth of the same cutting tool produced chip, but in different thicknesses (Figure 4.6 (a)) Comparing 1 and 20 µm run-outs of Nakanishi and Precise spindles, this is an expected result.

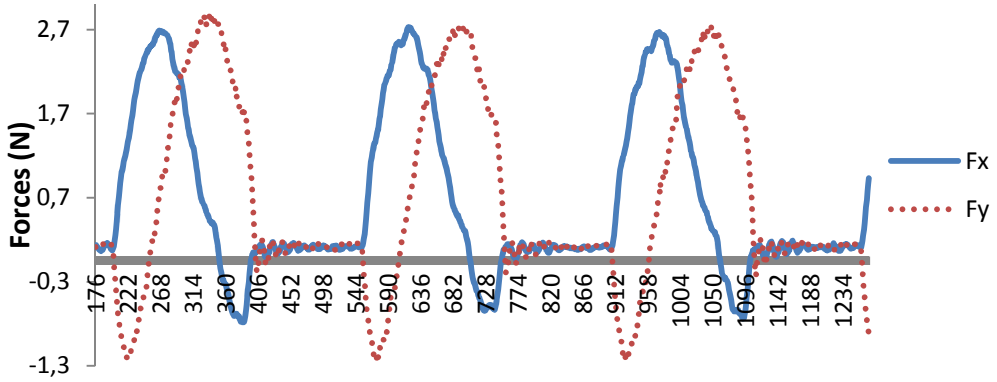

(a)

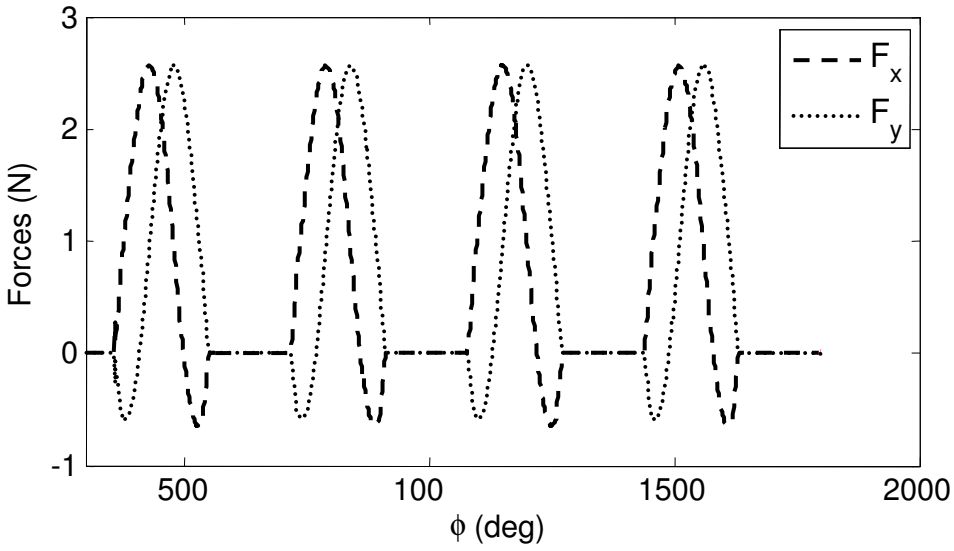

(b)

Figure 4.10: Instantaneous milling force values for Precise spindle with 17,000 rpm, 0.6 mm diameter cutting tool on Ti6Al4V workpiece with 2 µm/tooth feed rate and 0.12 mm depth of cut; a) measured and b) predicted.

Chapter 5

Conclusions and Future Works

In this study, modeling of micro milling forces is performed considering tool run-out and trochoidal tool path strategy. Mechanistic force modeling is modified to handle nonlinear average force variations as a function of feed. Micro milling force predictions showed a good agreement with the experimental data obtained during full immersion cutting tests on Ti6Al4V with micro tools of different diameters.

The thesis put a special focus on the spindle runout. Identical micro milling tests were performed with different spindles and it has been observed that spindle dynamics significantly affects the micro milling forces. But in this respect, statically measured run-out values can not be used in micro milling force modeling. Dynamic runout values are determined to be less than the static runout measurements. The reason behind this phenomenon is believed to be related to micro milling forces and the stiffness of the spindle-tool holder-tool system.

For future work;

- The minimum uncut chip thickness effect can be integrated into the model for better prediction performance at low feed machining cases.
- Elestic deformation of the cutting tool can be included in the model geometry. Furthermore, elastic deformation of the workpiece in the tertiary zone may be considered.

- The tool run-out can be measured dynamically. The results may be used to verify this model's prediction, that is revised by tool run-out and trochoidal tool path.
- Charts of cutting and edge force coefficients for some cutting conditions can be obtained via experimentation and this model.
- The model presented in this thesis can be extended to dynamic case.

Bibliography

[1] Budak E., Altintas Y. and Armarego E.J.A., Prediction of Milling Force Coefficients From Orthogonal Cutting Data, *Trans. ASME J. Manuf. Sci. Eng.*, 118 (2) (1996), pp. 216–224

[2] Wang J. J. Junz, Liang S. Y., Book W. J., Convolution Analysis of Milling Force Pulsation, *J. of Engineering for Industry* Vol. 116 (1994)

[3] Martellotti M. E., An Analysis of the Milling Process, *Transactions of the ASME*, Vol. 63 (1941), pp. 677-700.

[4] DeVor, R. E., and Kline, W. A., A Mechanistic Model for Machining Airframe Structures, *Proc. of the 8th North American Manufacturing Res. Conf.*, May 1980, p. 297.

[5] W.A.Kline, R.E.Devor, J.R.Lindberg, The prediction of cutting forces in end milling with application to cornering cut, *Int. J. Mach. Tools Manuf.* 22 (1) (1982) 7–22.

[6] Tlusty J. and MacNeil P., Dynamics of cutting forces in end milling, *CIRP Ann.* 24 (1975) 21–5.

[7] Usui E., Hirota A. and Masuko M., Analytical Prediction of Three Dimensional Cutting Process—Part 1: Basic Cutting Model and Energy Approach, *J. Manuf. Sci. Eng.* 100(2), 222-228 (1978)

[8] Usui E. and Hirota A., Analytical Prediction of Three Dimensional Cutting Process—Part 2: Chip Formation and Cutting Force with Conventional Single-Point Tool, *J. Manuf. Sci. Eng.* 100(2), 229-235 (1978)

[9] Fu H. J., DeVor R. E. and Kapoor S. G., A Mechanistic Model for the Prediction of the Force System in Face Milling Operations, *J. Manuf. Sci. Eng.. 1984; 106(1):81-88.*

[10] Smith S. and Tlusty J., An Overview of Modeling and Simulation of the Milling Process, *J. Manuf. Sci. Eng.* 113(2), 169-175 (1991) (7 pages)

[11] Armarego E. J. A. and Deshpande N.P., Computerized End-Milling Force Predictions with Cutting Models Allowing for Eccentricity and Cutter Deflections, *Annals of the CIRP* Volume 40, Issue 1 (1991), Pages 25–29

[12] Montgomery D. and Altintas Y., Mechanism of cutting force and surface generation in dynamic milling, *J. Eng. Ind.* 113 (1991) 160–8

[13] Armarego, E. J. A., and Deshpande, N. P., 1993, Force Prediction Models and CAD/CAM Software for Helical Tooth Milling Processes, Part I, Basic Approach and Cutting Analyses, Vol. 31, No. 8, pp. 1991-2009, Part II, Peripheral Milling Operations, Vol. 31, No. 10, pp. 2319-2336, Part III, Endmilling and Slotting Operations, in press, *International Journal of Production Research*.

[14] Armarego E. J. A., Wang J, Deshpande N P., Computer-aided predictive cutting model for forces in face milling allowing for tooth runout, *CIRP Annals — Manufacturing Technology*, 1995, 44(1): 3–48.

[15] Lee P., Altintas Y., Prediction-of-ball-end-milling-forces-from-orthogonal-cutting-data, *Int. J. Mach. Tools Manuf.*, 36 (1996), pp. 1059–1072

[16] Armarego E. J. A., The Unified-Generalized Mechanics Of Cutting Approach—A Step Towards A House Of Predictive Performance Models For Machining Operations, *Machining Science and Technology*, 4 , 3 (2000), pp. 319-362

[17] Kumanchik, L. M. and Schmitz, T.L., Improved analytical chip thickness model for milling, (2007) *Precision Engineering*, 31 (3), pp. 317-324

[18] Schmitz T. L., Couey J, Marshb E., Mauntler N. and Hughes D., Runout effects in milling: surface finish, surface location error, and stability, *Int J Mach Tools Manuf* 47(5) (2006):841–851

[19] Kaymakci, M., Kilic, Z. M. and Altintas, Y., Unified cutting force model for turning,boring, drilling and milling operations, *International Journal of Machine Tools and Manufacture* 54–55 2012, 34–45.

[20] Ber, A., and Feldman, D., A Mathematical Model of the Radial and Axial Throw of Square Indexable Inserts in Face Milling Cutter, *Annals of the CIRP*, Vol. 25 (1976), p. 19.

[21] Kline, W. A. and DeVor R. E., The Effect of Runout on Cutting Forces in End Milling, *International Journal of Machine Tool Design and Research*, Vol.23, no.2/3, 1983.

[22] Kim Jeong-Du and Kim Dong Sik, Theoretical analysis of micro-cutting characteristics in ultra-precision machining, *J. of Materials Processing Technology*, 49 (1995), 387-398

[23] Waldorf D. J. , DeVor R. E. and Kapoor S. G., A Slip-Line Field for Ploughing During Orthogonal Cutting, *J. Manuf. Sci. Eng.* 120(4), 693-699 (Nov 01, 1998)

[24] Bao, W.Y., Tansel, I.N., Modeling micro-end-milling operations. Part I: Analytical cutting force model**,** (2000) *International Journal of Machine Tools and Manufacture*, 40 (15), pp. 2155-2173

[25] Bao, W.Y., Tansel, I.N., Modeling micro-end-milling operations. Part II: Tool run-out**,** (2000) *International Journal of Machine Tools and Manufacture*, 40 (15), pp. 2175-2192.

[26] Bao, W.Y., Tansel, I.N., Modeling micro-end-milling operations. Part III: Influence of tool wear, (2000) *International Journal of Machine Tools and Manufacture* 40 (15) PP. 2193 – 2211

[27] Vogler Michael P., DeVor Richard E. and Kapoor Shiv G., Microstructure-Level Force Prediction Model for Micro-milling of Multi-Phase Materials, *Journal of Manufacturing Science and Engineering-transactions of The Asme*, Volume 125 (2003), 202-209

[28] Dow Thomas A., Miller Edward L. and Garrard Kenneth, Tool force and deflection compensation for small milling tools, *Precision Engineering*, 28 (2004,) 31–45

[29] Kim Chang-Ju, Mayor J. Rhett and Ni Jun, A Static Model of Chip Formation in Microscale Milling, *Journal of Manufacturing Science and Engineering-transactions of The Asme*, Volume 126 (2004), 710-718

[30] Li H.Z. and Li X.P., A numerical study of the effects of cutter runout on milling process geometry based on true tooth trajectory, *Int J Adv Manuf Technology* (2005) 25: 435–443

[31] Wan M. and Zhang W.H., Calculations of chip thickness and cutting forces in flexible end milling, *Int. J Adv Manuf Technology* (2005) 00: 1–11

[32] Chae J., Park S.S. and T. Freiheit, Investigation-of-micro-cutting-operations, *International Journal of Machine Tools & Manufacture* 46 (2006) 313–332

[33] Dhanorker Atul and Özel Tuğrul, An experimental and modeling study on meso-micro end milling process, *Proceedings of 2006 ASME International Conference on Manufacturing Science and Engineering*, Paper No. 21127

[34] Li Chengfeng, Lai Xinmin, Li Hongtao and Ni Jun, Modeling of three-dimensional cutting forces in micro-end-milling, *J. Micromech. Microeng.* 17 (2007) 671–678

[35] Kang I.S., Kim J.S., Kang M.C. and Seo Y.W., A mechanistic model of cutting force in the micro end milling process, *Journal of Materials Processing Technology* 87-188 (2007) 250-255

[36] Jun Martin B.G., Bourne Keith, DeVor Richard E. and Kapoor Shiv G., Estimation of effective error parameters in high-speed micro-endmilling, *International Journal of Machine Tools & Manufacture* 47 (2007) 1449–1454

[37] Lai Xinmin, Li Hongtao, Li Chengfeng, Lin Zhongqin and Ni Jun, Modelling and analysis of micro scale milling considering size effect, micro cutter edge radius and minimum chip thickness, *International Journal of Machine Tools & Manufacture* 48 (2008) 1–14

[38] Malekian Mohammad, Park Simon S. and Jun Martin B.G., Modeling of dynamic micro-milling cutting forces, *International Journal of Machine Tools & Manufacture* 49 (2009) 586–598

[39] Park S.S. and Malekian M., Mechanistic modeling and accurate measurement of micro end milling forces, *CIRP Annals - Manufacturing Technology* 58 (2009) 49–52

[40] Wyen C.-F. and Wegener Konrad "Influence of cutting edge radius on cutting forces in milling titanium" *CIRP Annals - Manufacturing Technology* 59 (2010) 93–96

[41] Afazov S.M., Ratchev S.M.and Segal J., Modelling and simulation of micro-milling cutting forces, *Journal of Materials Processing Technology* 210 (2010) 2154–2162

[42] *http://www.micromanufacturing.net/didactico/Desarollo/micromilling*

[43] Germain Dimitri, Fromentin Guillaume, Poulachon Gerard and Bissey-Breton Stephanie, From large-scale to micromachining: A review of force prediction models, Journal of Manufacturing Processes 15 (2013) 389–401

[44] *http://www.precisebits.com/tutorials/tir.htm*

[45] *http://www.ns-tool.com*

[46] *http://www.keyence.com/products/microscope/high-speed-microscope/vw-9000/index.jsp*

Appendix

Matlab Codes

A. Codes for Force Coefficients (Linear Fit)

```
a=1;
Nt=2;                          % number of teeth, int
phis = 0;                        % cut start angle, deg
phie = 180;                       % cut exit angle, deg

P=(a*Nt/2/pi)*(cos(2*phie*pi/180)-cos(2*phis*pi/180));
Q=(a*Nt/2/pi)*(2*(phie*pi/180-phis*pi/180)-(sin(2*phie*pi/180)-
sin(2*phis*pi/180)));
S=(a*Nt/2/pi)*(sin(phie*pi/180)-sin(phis*pi/180));
T=(a*Nt/2/pi)*(cos(phie*pi/180)-cos(phis*pi/180));

% for d=2mm cutter,     10,000rpm,  doc=0.2mm
  Fxc=95.136;  Fxe=26.447;  Fyc=1227.8;  Fye=9.8507;

% for d=2mm cutter, 14,000rpm, doc=0.2mm
  Fxc=484.17;  Fxe=22.617;  Fyc=1272.1;  Fye=10.112;

% for d=0.6mm cutter,   17,000rpm,  doc=0.12mm
% Fxc=761.58;  Fxe=9.457;  Fyc=1410.2;  Fye=5.7959;   %

% for d=0.4mm cutter,   26,000rpm,  doc=0.08mm
% Fxc=969.8;  Fxe=7.0513;  Fyc=1379.6;  Fye=5.2798;   %

% cutting and edge force coeffications
Kte= ((Fxe*S - Fye*T)/(S^2 + T^2))       % tangential specific
force, N/mm^2
Ktc= (4*(Fyc*Q - Fxc*P)/(P^2 + Q^2))
Kre= ((Kte*S - Fxe)/ T )                 % normal specific
force, N/mm^2
Krc= ((Ktc*P + 4*Fxc)/ Q)
```

B. Codes for Force Coefficients (Polynomial Fit)

```
a=1;
Nt=2;                          % number of teeth, int
phis = 0;                      % cut start angle, deg
phie = 180;                    % cut exit angle, deg


A=(a*Nt/2/pi)*(cos(phie*pi/180)-cos(phis*pi/180));
B=(a*Nt/2/pi)*(sin(phie*pi/180)-sin(phis*pi/180));
C=(a*Nt/2/pi)*(2*(phie*pi/180-phis*pi/180)-(sin(2*phie*pi/180)-
sin(2*phis*pi/180)));
D=(a*Nt/2/pi)*(cos(2*phie*pi/180)-cos(2*phis*pi/180));
E=(a*Nt/2/pi)*((cos(3*phie*pi/180)-cos(3*phis*pi/180))-
9*(cos(phie*pi/180)-cos(phis*pi/180)));
F=(a*Nt/2/pi)*(sin(phie*pi/180)^3-sin(phis*pi/180)^3);
G=(a*Nt/2/pi)*(12*(phie*pi/180-phis*pi/180)-
8*(sin(2*phie*pi/180)-sin(2*phis*pi/180))+sin(4*phie*pi/180)-
sin(4*phis*pi/180));
H=(a*Nt/2/pi)*(sin(phie*pi/180)^4-sin(phis*pi/180)^4);

% for d=0.4mm cutter,   26,000rpm,  doc=0.08mm  Nakanishi 0.4
Fx3=4e7; Fx2=-839557; Fx1=5780.4; Fx0=0;
Fy3=3e7; Fy2=-616773; Fy1=4953.3; Fy0=0;

% specific force coeffications
Kt0= (Fx0*B - Fy0*A)/(B^2 + A^2)      % tangential specific
force, N/mm^2
Kr0= (Fy0*B - Fx0*A)/(B^2 + A^2)      % normal specific force,
N/mm^2
Kr1= 4*(Fy1*D + Fx1*C)/(D^2 + C^2)
Kt1= 4*(Fy1*C - Fx1*D)/(D^2 + C^2)
Kt2= 12*(Fy2*E + 4*Fx2*F)/(E^2 + 16*F^2)
Kr2= 12*(Fx2*E - 4*Fy2*F)/(E^2 + 16*F^2)
Kt3= 32*(Fy3*G + 8*Fx3*H)/(G^2 + 64*H^2)
Kr3= 32*(Fx3*G - 8*Fy3*H)/(G^2 + 64*H^2)
```

C. Codes for Instantaneous Force Calculation

```
Ktc= 2455.6;     Kte= 15.47;    Krc= 190.27;    Kre= 41.54;  %
10,000rpm,

%Milling Parameters
b = 0.200;                          % axial depth, mm
ft = 0.004;                         % feed per tooth, mm/tooth
gamma = 30;                        % helix angle, deg
d = 2;                            % cutter diameter, mm
Nt=2;                              % number of teeth
omega = 10000;           % spindle speed, rpm
%%%%%%%%%%%%%%%%%%%%%%
%Tool run out specs
ro=0.004;              % radyus of run-out, mm
gama=45*pi/180;          % angle of run-out, rad
r0=(d/2);
r1=(d/2);
%%%%%%%%%%%%%%%%%
duration=2*pi*3;  %3 full rotation
steps=684;
dphi=duration/steps;
%%%%%%%%%%%%%%%%%%%%%%%%%%%%%%%%%%%%%%%%%%%%%%%%
if gamma == 0                      % straight teeth
    db = b;                        % discretized axial depth, m
else                               % nonzero helix angle
    db = d*(dphi)/2/tan(gamma*pi/180);
end
kappa=db*tan(gamma*pi/180)/(d/2);

steps_axial = round(b/db);      % number of steps along tool
axis

%%%%%%%%%%%%%%%%%%%%%%%%%%%%%%%%%%%%%%%%%%%%%%%%%%%%%%%%%%%
tooth_angles = 0:360/Nt:(360-360/Nt);  % angles of Nt cutter
teeth starting from zero, deg
phi = linspace(0, duration,steps);
%%%%%%%%%%%%%%%%%%%%%%%%%%%%%%%%%%%%%%%%%%%%%%%%%%%%%%%%%%%%%%%%%%%

for i=1:steps
    Fx=0;
    Fy=0;

    for cnt4 = 1:steps_axial
    phix=phi(i)-(cnt4-1)*kappa;

[h0,h1,x0,y0,x1,y1,phis]=chipthicknesswithrunout2(ro,gama,r0,r1
,ft,phix);
    h0x(i)=h0;
    h1x(i)=h1;
```

```
    x0(i)=x0;
    y0(i)=y0;
    x1(i)=x1;
    y1(i)=y1;

    if h0>=0 && h1<0
    h(i)=h0;
    elseif h1>=0 && h0<0
    h(i)=h1;
        end

    if h0>=0 && h1<0
                Ft=db*h0*Ktc+db*Kte;
                Fn=db*h0*Krc+db*Kre;
                Fx = Fx + Fn*sin(phix) + Ft*cos(phix);    % N
                Fy = Fy - Fn*cos(phix) + Ft*sin(phix);    % N
    elseif h1>=0 && h0<0
                Ft=db*h1*Ktc+db*Kte;
                Fn=db*h1*Krc+db*Kre;
                Fx = Fx + Fn*sin(phis) + Ft*cos(phis);    % N
                Fy = Fy - Fn*cos(phis) + Ft*sin(phis);    % N
    end
    end

    Force_x(i) = Fx;
    Force_y(i) = Fy;

end

figure (8)
plot(phi*180/pi, h, 'k-', 'LineWidth',2)
set(gca,'FontSize', 14)
xlabel('\phi (deg)')
ylabel('h (mm)')
legend('Uncut Chip Thickness')
```